Targeting and imaging single biomolecules in living cells by complementation-activated light microscopy with split-fluorescent proteins

Fabien Pinaud[1] and Maxime Dahan

Laboratoire Kastler Brossel, Centre National de la Recherche Scientifique Unité de Recherche 8552, Physics Department and Institute of Biology, Ecole Normale Supérieure, Université Pierre et Marie Curie-Paris 6, 75005 Paris, France

Single-molecule (SM) microscopy allows outstanding insight into biomolecular mechanisms in cells. However, selective detection of single biomolecules in their native environment remains particularly challenging. Here, we introduce an easy methodology that combines specific targeting and nanometer accuracy imaging of individual biomolecules in living cells. In this method, named complementation-activated light microscopy (CALM), proteins are fused to dark split-fluorescent proteins (split-FPs), which are activated into bright FPs by complementation with synthetic peptides. Using CALM, the diffusion dynamics of a controlled subset of extracellular and intracellular proteins are imaged with nanometer precision, and SM tracking can additionally be performed with fluorophores and quantum dots. In cells, site-specific labeling of these probes is verified by coincidence SM detection with the complemented split-FP fusion proteins or intramolecular single-pair Förster resonance energy transfer. CALM is simple and combines advantages from genetically encoded and synthetic fluorescent probes to allow high-accuracy imaging of single biomolecules in living cells, independently of their expression level and at very high probe concentrations.

biomolecular imaging | membrane biophysics | single-molecule fluorescence | single-particle tracking | high-resolution microscopy

In recent years, parallel developments in imaging technologies, optical probes, and genetic engineering have contributed to the fast emergence of single molecule (SM) fluorescence techniques. These techniques now permit the imaging of subcellular structures with nanometer resolution and tracking of individual proteins as well as stochiometric analysis of molecular complexes in living cells (1, 2). A key requirement for SM microscopy is to limit the number of biomolecules that are simultaneously imaged to maintain an SM detection regimen while recording a statistically representative number of events. Hence, advanced labeling and targeting strategies are needed to ensure specific and sensitive detection of individual biomolecules in complex cellular environments.

In situ, protein labeling can be achieved by incorporating molecular tags that are posttranslationally coupled to exogenous fluorophores (3) or fusion to fluorescent proteins (FPs) (4). Posttranslational labeling of molecular tags necessitates probe concentrations in the micromolar range (3), well above the typical subnanomolar range required for SM imaging. Such high concentrations increase the risks of nonspecific binding in cells, impose extensive washing of the nontargeted probes, and complicate SM detection. When using FPs, low expression levels required for SM imaging are often difficult to achieve, and high expressions demand potentially toxic photobleaching. Some of these issues can be alleviated by using switchable fluorescent probes that permit low background and controlled imaging of only a fraction of tagged biomolecules in live cells (5–7). The growing panel of photoswitchable FPs is particularly useful, because it does not require advanced cellular targeting chemistries

(8). However, genetically encoded FPs are neither as bright nor as photostable as the best organic and inorganic fluorophores.

Split-FPs are another type of genetically encoded fluorescent probes that switch on when reconstituted. They have been extensively used to study protein interactions in living cells by bimolecular fluorescence complementation (BiFC) (9). In BiFC assays, two proteins of interest are fused to two nonfluorescent FP fragments of roughly equal size, and protein–protein interaction drives the complementation of the fragments into a fluorescent FP. Recently, a highly asymmetric split-GFP based on a super-folder GFP was engineered in a large GFP 1–10 fragment (amino acids 1–214) and a small GFP 11 peptide fragment corresponding to the 11th β-strand of the super-folder GFP β-barrel (amino acids 214–230) (10). Both fragments spontaneously self-complement in solution, and the GFP 11 fragment can be mutated for fast complementation (11) or produced synthetically for in vitro complementation with GFP 1–10 (12, 13). When used as protein tags, GFP 11 and GFP 1–10 helped visualize synaptic contacts and distribution of bacterial effectors in cells (14, 15).

Here, we have exploited several aspects of this asymmetric split-GFP system to target, image, and track individual proteins in living cells. We have developed complementation-activated light microscopy (CALM), an SM imaging methodology that relies on the irreversible and stochastic complementation of GFP 1–10 fusion proteins by synthetic versions of the GFP 11 peptide fragment. In living cells, a controlled subset of proteins fused to GFP 1–10 is activated into bright GFPs and continuously imaged by simply adjusting the concentrations and incubation times with engineered peptides. Using CALM, low-background and ultra-specific tracking of individual transmembrane, GPI-anchored, or caveolae-associated proteins was achieved in various cell lines within minutes of peptide addition. We also used CALM for site-directed posttranslational targeting of synthetic and fluorescent moieties to individual proteins. In living cells, specific and stochiometric labeling using single fluorophores and quantum dots (qdots) was verified by coincident SM detection with the complemented split-FP fusion proteins and allowed for advanced bioimaging modalities. For instance, when combining CALM and single-pair Förster resonance energy transfer (spFRET) from a complemented GFP to an acceptor peptide conjugate, single proteins could be tracked independently of their expression level and at probe concentrations in the micromolar range.

Results

In Vitro Bulk Complementation of Split-GFP with Small Synthetic Peptides. We first tested the complementation of GFP 1–10 with a variety of small synthetic peptides containing a mutated version of the GFP 11 fragment referred to as M3 peptides (Fig. 1*A*). We designed a 24-aa complementary peptide with an N-terminal biotin and a flexible linker to the C-terminal M3 sequence (biotin-M3) and verified its in vitro complementation with soluble GFP 1–10. Neither GFP 1–10 nor the synthetic biotin-M3 peptide is fluorescent but they self-assemble into a complemented, bright, and monomeric GFP-biotin with an apparent molecular weight (MW) of 25.0 kDa (Fig. 1*B* and *SI Appendix,* Fig. S1). Binding of

M3 peptides to GFP 1–10 and GFP complementation was also tested with fluorescently labeled M3 peptides. On incubation with GFP 1–10, M3 peptides conjugated to the Alexa 647 fluorophore (M3-A647; >97% purity) (*SI Appendix,* Fig. S2) were shifted on native gels compared with Alexa 647 alone or unreacted M3-A647 (Fig. 1*C*). Specific binding of M3-A647 to GFP 1–10 and GFP complementation was confirmed by the appearance of a colocalizing GFP fluorescence band and competition with excess nonfluorescent biotin-M3 peptides (Fig. 1*C*). Similar results were obtained by size-exclusion chromatography (*SI Appendix,* Fig. S1).

In solution, the complementation kinetics of GFP 1–10 with synthetic M3 peptides were fast and spread over a 2-h period
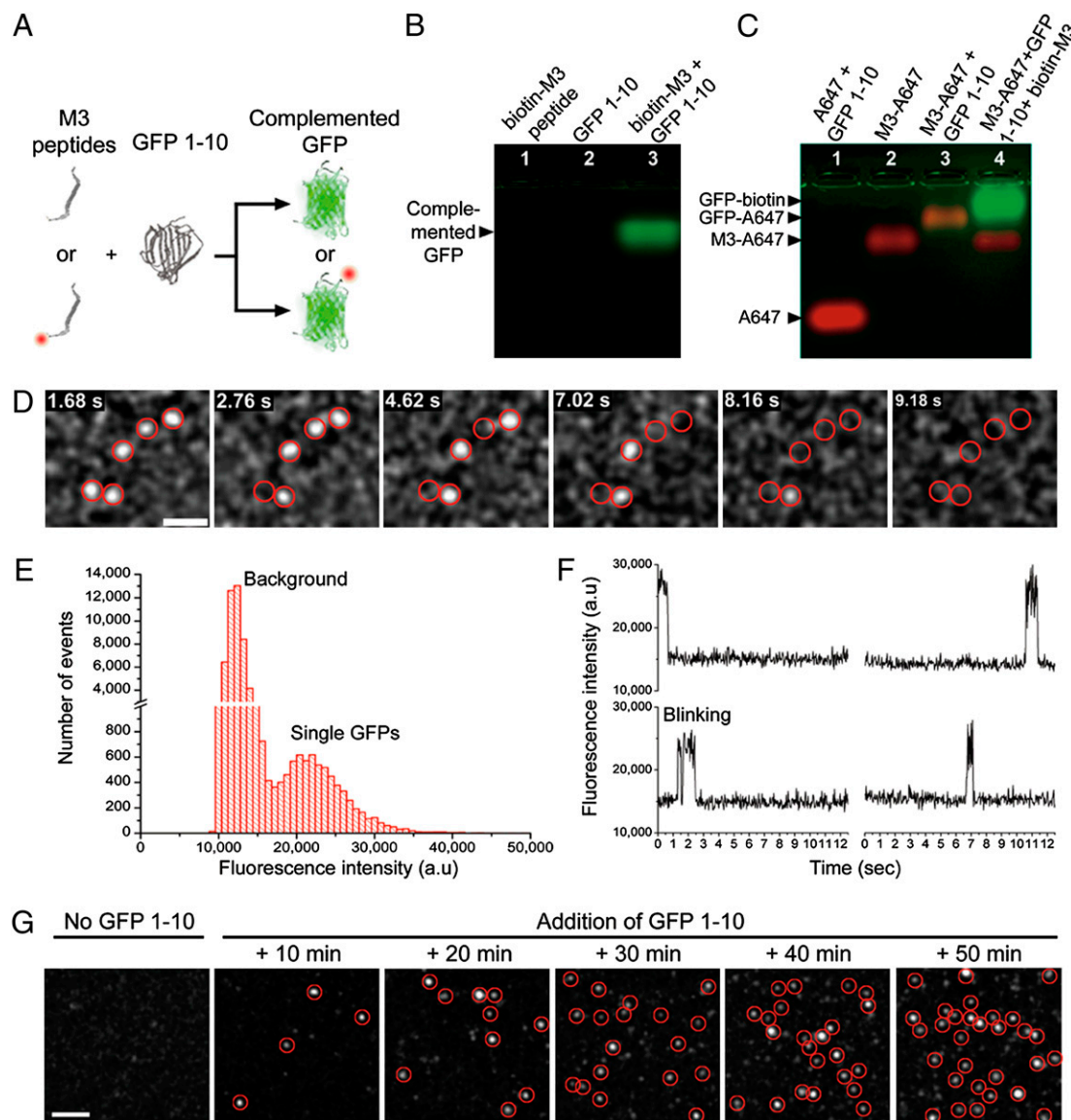
Fig. 1. Complementation of GFP 1–10 with synthetic M3 peptides and in vitro SM imaging. (*A*) Schematic of self-complementation between nonfluorescent (*Upper*) and fluorescent (*Lower*) synthetic M3 peptides and GFP 1–10. (*B*) Native gel electrophoresis of biotin-M3 peptide (lane 1), GFP 1–10 (lane 2), and complementation reaction of biotin-M3 with GFP 1–10 (lane 3). (*C*) Native gel shift of free Alexa 647 (A647; lane 1), unreacted M3-Alexa 647 conjugate (M3-A647; lane 2), and M3-A647 reaction with GFP 1–10 in the absence (lane 3) or presence (lane 4) of a competing excess of biotin-M3 peptides. (*D*) Sequential photobleaching of complemented and purified individual GFP-biotin nonspecifically bound to a glass coverslip and imaged by TIRF (Movie S1). GFP diffraction-limited spots are intentionally expanded to facilitate visualization. (Scale bar: 2 μm.) (*E*) Fluorescence intensity distribution for 152 single-complemented GFP-biotin molecules and background fluorescence from coverslips. (*F*) Fluorescence time traces of four single split-GFPs complemented on M3 peptide-coated coverslips. Single-step photobleaching and blinking events are observed. (*G*) Representative TIRF fields of view taken at different incubation times before and after addition of GFP 1–10 to M3 peptide-coated coverslips. The number of individual-complemented GFP-biotin per fields of view increases with increasing incubation times. GFP diffraction-limited spots are intentionally expanded to facilitate visualization. (Scale bar: 2 μm.)

before reaching saturation (*SI Appendix*, Fig. S3). Consistent with previous results (10), GFP fluorescence resulting from the complementation scaled linearly with the concentration of peptides under nonsaturating conditions.

To further assess the flexibility of our designed peptides and evaluate the complementation efficiency under restricted conformational freedom, two biotinylated M3 sequences were affixed to streptavidin-coated agarose beads. As for solution-based assays, the beads rapidly became fluorescent when incubated with GFP 1–10 (*SI Appendix*, Fig. S4), indicating that surface attachment did not sterically hinder the complementation.
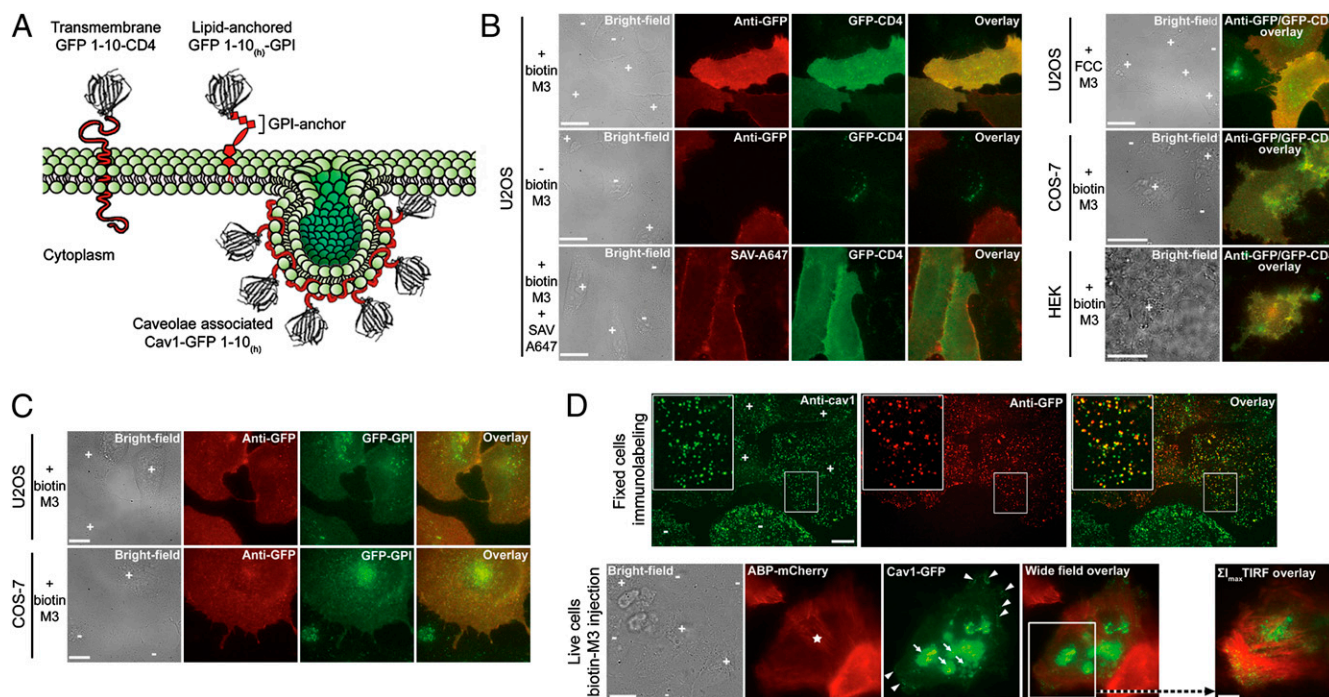
In Vitro SM Imaging of Split-GFP Complementation. Next, we tested our ability to detect single GFP copies complemented by M3 peptides. GFP 1–10 in bacterial extract was incubated with biotin-M3, purified by high-pressure liquid chromatography (HPLC), and diluted solutions of complemented GFP-biotin deposited on glass coverslips were imaged by total internal reflection fluorescence (TIRF) microscopy. Diffraction-limited fluorescence spots corresponding to single complemented GFP-biotin were detected (Fig. 1*D*). The single emitter nature of GFP-biotin molecules was confirmed by their unimodal fluorescence intensity distribution (Fig. 1*E*), their single-step photobleaching, and blinking events (Fig. 1*F* and Movie S1).

Single GFPs could also be detected during the complementation process. M3-biotin peptides were affixed to avidin-functionalized coverslips and imaged by TIRF while incubating

coverslips with GFP 1–10. In the absence of GFP 1–10, no fluorescence was detected, but single diffraction-limited spots of complemented GFP-biotin appeared at the coverslip surface within 10 min of incubation (Fig. 1*G*). The number of single GFPs per field of view increased over time, which is in agreement with the solution-based complementation kinetic assays. Sudden appearances of single GFPs during imaging were also observed (Fig. 1*F*), clearly indicating that the complementation of single split-GFPs could be directly imaged.

Live Cell CALM Imaging of Split-GFP Fusion Proteins. To evaluate if CALM would be similarly efficient in living cells, we expressed GFP 1–10 as an N- or C-terminal fusion to extracellular and intracellular membrane proteins in different mammalian cell lines (Fig. 2*A*). As extracellular proteins, we used two membrane raft-associated proteins, a transmembrane CD4 split-GFP fusion (14) (GFP 1–10-CD4), and a glycosylphosphatidyl inositol (GPI)-anchored humanized split-GFP fusion (GFP 1–10$_{(h)}$-GPI) attached to the upper leaflet of the plasma membrane. As an intracellular protein, we fused GFP 1–10$_{(h)}$ to caveolin-1 (cav1-GFP 1–10$_{(h)}$), an integral membrane protein participating in the scaffolding of 50- to 100-nm caveolae invaginations at the plasma membrane (16).

When expressed in U2OS, COS-7, and HEK cells, GFP 1–10-CD4 and GFP 1–10$_{(h)}$-GPI were properly directed to the plasma membrane, which was verified by live cell labeling with anti-GFP antibodies recognizing GFP 1–10 (Fig. 2 *B* and *C*). Their mem-

Fig. 2. CALM imaging in living cells. (*A*) Schematic representation of plasma membrane split-GFP fusions used in this work. (*B*) Wide-field fluorescence imaging of GFP 1–10-CD4 expression and complementation in U2OS, COS-7, and HEK cells. Expressing cells (+) are detected with a fluorescent anti-GFP antibody. When incubated with M3 peptides (+biotin-M3 or +FCC-M3), GFP 1–10-CD4 proteins are activated into bright GFP-CD4 proteins, and expressing cells become fluorescent (overlay). No GFP signal is seen in the absence of peptides (–biotin-M3) or for nonexpressing cells (–). Binding of the complementary biotin-M3 peptides on the cell surface is verified by staining with fluorescent streptavidin (SAV-A647). (Scale bar: 20 μm.) (*C*) Wide-field fluorescence imaging of GFP 1–10$_{(h)}$-GPI expression and complementation in U2OS and COS-7 cells. (Scale bar: 10 μm.) (*D*) Fluorescence confocal, wide-field, and TIRF imaging of cav1-GFP 1–10$_{(h)}$ expression and intracellular complementation in U2OS cells. (*Upper*) Ventral plasma membrane confocal images of fixed cells immunolabeled for endogenous cav1 (anti-cav1) and cav1-GFP 1–10$_{(h)}$ (anti-GFP) showing cav1-GFP 1–10$_{(h)}$ colocalization with endogenous cav1 (overlays and *Insets*). 3D reconstructions of cells are available in Movie S4. (Scale bar: 20 μm.) (*Lower*) Fluorescence wide-field imaging of live U2OS cells coexpressing cav1-GFP 1–10$_{(h)}$ and ABP-mCherry (+). A cell microinjected with M3 peptides (star; ~25 μM final intracellular M3 peptide concentration) and imaged after 45 min incubation at 37 °C shows a perinuclear pool of complemented cav1-GFP$_{(h)}$ (arrows) and a plasma membrane pool of caveolae-associated cav1-GFP$_{(h)}$ (arrowheads). The typical punctuated pattern of complemented caveolae is better seen by TIRF imaging of the plasma membrane (white square). The TIRF image is a pixel-based maximum intensity projection (ΣI_{max}) overlay image for all frames of the dual-color Movie S5. (Scale bar: wide-field, 10 μm; TIRF, 5 μm.)

brane distribution was homogenous, with no aggregation or mislocalization. On incubation with high concentrations of M3 peptides (50 μM) for 45–60 min, GFP fluorescence was specifically detected at the membrane of transfected cells (Fig. 2 *B* and *C*), which was confirmed by confocal and TIRF imaging (*SI Appendix*, Fig. S5 and Movie S2). The appearance of the GFP signal was solely triggered by the complementation reaction, because no GFP fluorescence was observed for nontransfected cells or when M3 peptides were omitted (Fig. 2*B* and *SI Appendix*, Fig. S5). Specific binding of M3 peptides to GFP 1–10 fusion proteins was further established by incubating cells with biotin-M3 and observing colocalized membrane signals from GFP and a fluorescently labeled streptavidin (SAV-A647) (Fig. 2*B*). At the membrane, GFP signal was uniform and proportional to the membrane expression level of GFP 1–10-CD4 and GFP 1–10$_{(h)}$-GPI as implied by the equivalent intensity ratios between anti-GFP and GFP fluorescence in different cells (Fig. 2*B*). Consistent with in vitro complementation kinetics assays, long incubations of M3 peptides with expressing cells resulted in increased total GFP signal, and intense fluorescence was detected after 48 h incubation (Movie S3).

Intracellular expression and association of cav1-GFP 1–10$_{(h)}$ with caveolae were verified by double immunolabeling of U2OS cells with anti-cav1 and anti-GFP antibodies. The typical punctuated membrane pattern of caveolae-associated endogenous cav1 (17, 18) colocalized with that of cav1-GFP 1–10$_{(h)}$ (Fig. 2*D* and Movie S4) for transfected cells, indicating that functional cav1-GFP 1–10$_{(h)}$ fusion proteins contribute together with endogenous cav1 to the formation of membrane caveolea in U2OS cells.

Intracellular complementation of cav1-GFP 1–10$_{(h)}$ was then tested by direct microinjection of M3 peptides in live and expressing U2OS cells identified with the coexpression marker actin-binding peptide mCherry-LifeAct (ABP-mCherry). Cells became GFP-fluorescent when microinjected with a high concentrations of M3 peptides (∼25 μM final intracellular concentration) followed by 45 min incubation (Fig. 2*D*). In wide-field fluorescence images, a perinuclear pool of cav1-GFP$_{(h)}$ was detected together with the typical punctuated pattern of caveolae-associated cav1-GFP$_{(h)}$ at the plasma membrane (Fig. 2*D*). Complemented and GFP-fluorescent caveolae were clearly visible when the cell membrane was imaged by TIRF microscopy (Fig. 2*D* and Movie S5). No GFP fluorescence was observed for nonexpressing or noninjected cells (Movie S5).

Single Biomolecule Imaging in Living Cells by CALM. Making use of the concentration and time-dependant complementation kinetics of GFP 1–10, an SM detection regimen where individual split-GFP fusion proteins were continuously activated, imaged, and photobleached could easily be attained using low concentrations of M3 peptides. For this, the ventral plasma membrane of cells stably expressing GFP 1–10-CD4 or GFP 1–10$_{(h)}$-GPI proteins was repeatedly imaged by TIRF for 1 min in 5-min intervals before and during the addition of 1.8 μM M3 peptides. Before addition of the peptides, rare spurious SM events corresponding to cellular or imaging media materials emitting fluorescence at 520 nm were detected (typically less than 3% of all detected events). A few diffraction-limited GFP spots were immediately detected on addition of biotin-M3 to cells, and lateral membrane diffusion of individual complemented GFP-CD4 proteins was clearly observed within 5 min of incubation (Fig. 3*A* and Movie S6) as confirmed by single-step photobleaching and blinking events. The number of single GFP-CD4 detected steadily increased during the first 10–15 min and remained relatively constant at longer incubation times (Fig. 3*A* and Movie S6) in line with in vitro complementation kinetic assays. On addition of 10-fold more biotin-M3 (18 μM), a higher number of GFP-CD4 appeared at the cell membrane (Fig. 3*B* and Movie S6), but GFP spots were still sufficiently separated to clearly identify individual

biomolecules (Fig. 3*A*). No GFP signal was detected for nonexpressing cells imaged with similar peptide concentrations and incubation times (Movie S6). Thus, regardless of the protein expression levels, single biomolecules could easily be imaged in living cells by relying on the stochastic binding of M3 peptides and activation of split-GFP fusion proteins.

The high signal to background obtained by lighting up single GFP-CD4 in the otherwise dark cell membrane enabled the precise localization and tracking of individual CD4 with a mean uncertainty of 24 ± 4 nm (Fig. 3 *C* and *D* and *SI Appendix*, Table S1). Their apparent diffusion coefficient calculated from ensemble mean square displacements (MSD) was 0.21 ± 0.03 μm²/s, which is in good agreement with coefficients expected for transmembrane proteins in cells (*SI Appendix*, Table S1 and *SI Appendix*, Fig. S6). A more detailed analysis by probability distribution of the square displacements (P_r^2) (19) revealed that the coefficient derived from MSD actually comprises two GFP-CD4 subpopulations differing by about 10-fold in their diffusion coefficients: 0.29 ± 0.02 μm²/s (64%) and 0.021 ± 0.009 μm²/s (36%), respectively (*SI Appendix*, Table S1). These two subpopulations are consistent with the putative dynamic partitioning of CD4 into membrane raft microdomains (20, 21).

Similar tracking experiments were successfully carried out for individual GFP 1–10$_{(h)}$-GPI fusion proteins, which diffused two times faster than GFP-CD4 as expected for lipid-anchored plasma membrane proteins (0.37 ± 0.02 μm²/s) (*SI Appendix*, Table S1 and Figs. S6 and S7 and Movie S7). As for GFP-CD4, P_r^2 analysis revealed two diffusing subpopulations of GFP$_{(h)}$-GPI proteins, with diffusion coefficients of 0.53 ± 0.03 μm²/s (69%) and 0.036 ± 0.008 μm²/s (31%), respectively. These fast and slow subpopulations are fully consistent with the dynamic partitioning of this GPI-anchor in and out of membrane raft microdomains previously observed in HeLa cells (22).

Single cav1-GFP 1–10$_{(h)}$ could also be imaged by CALM inside living cells. Expressing cells identified by coexpression of a nucleus-localized CFP-LacI-NLS marker were microinjected with biotin-M3 (∼5 μM final intracellular concentration) and biotin-Alexa 647, used here as a microinjection marker (Fig. 4*A*). As an alternative to microinjection, M3 complementary peptides were efficiently translocated to the cell cytoplasm using cell penetrating Pep-1 peptides (23) and simple addition to the cell media (*SI Appendix*, Fig. S8). Within minutes, single diffraction-limited GFP spots of complemented cav1-GFP$_{(h)}$ were detected by TIRF at the ventral plasma membrane, and an increasing number of individual cav1-GFP$_{(h)}$ lit up with increasing incubation times (Fig. 4*B* and Movie S8). No GFP fluorescence was observed for noninjected cells expressing cav1-GFP 1–10$_{(h)}$ or microinjected cells that did not express the fusion protein (Fig. 4*B* and *SI Appendix*, Fig. S9). Single membrane-anchored cav1-GFP$_{(h)}$ could be tracked with a mean localization uncertainty of 14 ± 4 nm (Fig. 4 *C* and *D* and *SI Appendix*, Table S1) and diffused with an apparent ensemble MSD diffusion coefficient of 0.02 ± 0.003 μm²/s. P_r^2 analysis further indicated that a very slow and dominant subpopulation of caveolae-associated cav1-GFP$_{(h)}$ (0.002 ± 0.001 μm²/s, 74%) was present together with a faster-diffusing second subpopulation (0.059 ± 0.009 μm²/s, 26%) at the plasma membrane. These values are in excellent agreement with ensemble and caveolae-specific fluorescence recovery after photobleaching (FRAP) measurements of cav1 diffusion in the plasma membrane of a variety of other cells lines (24).

Thus, by fine-tuning the concentration of complementary peptides and their incubation time with cells, CALM allowed rapid, controllable, and highly specific detection and tracking of single biomolecules in living cells.

Split-GFPs as Posttranslational Protein-Targeting Platforms in Living Cells. Gel electrophoresis assays, (Fig. 1 and *SI Appendix*, Fig. S11), live cell imaging (Fig. 2*B*), and additional fluorescence
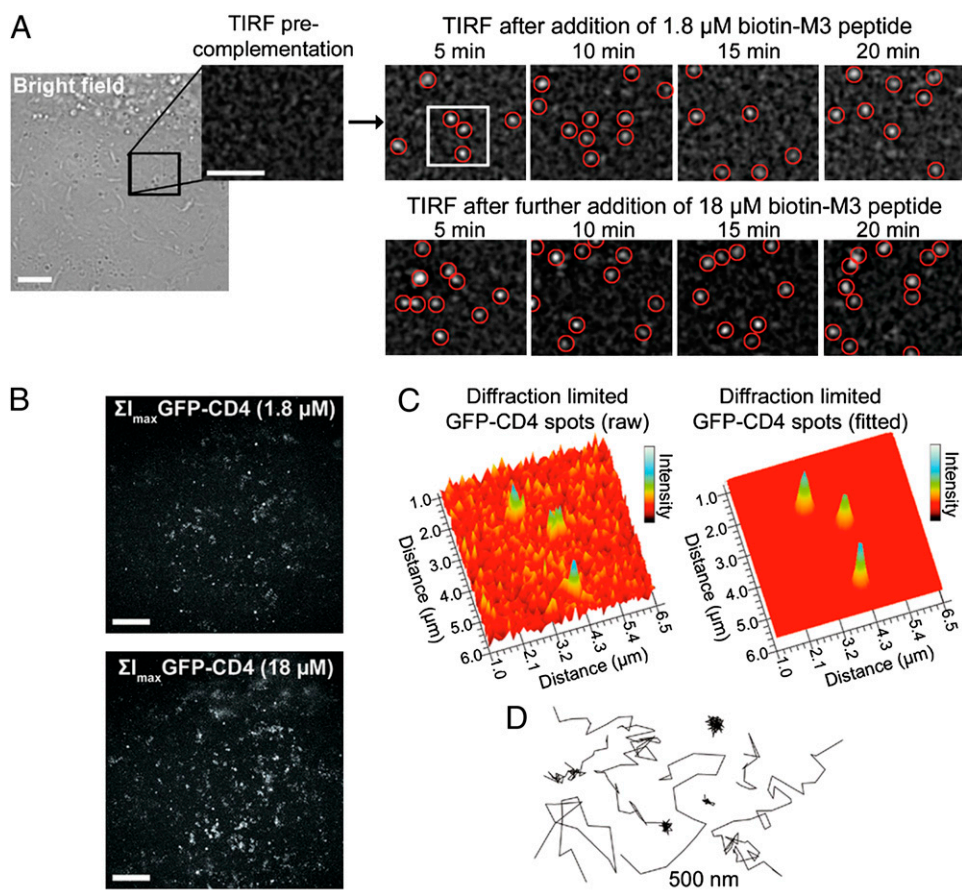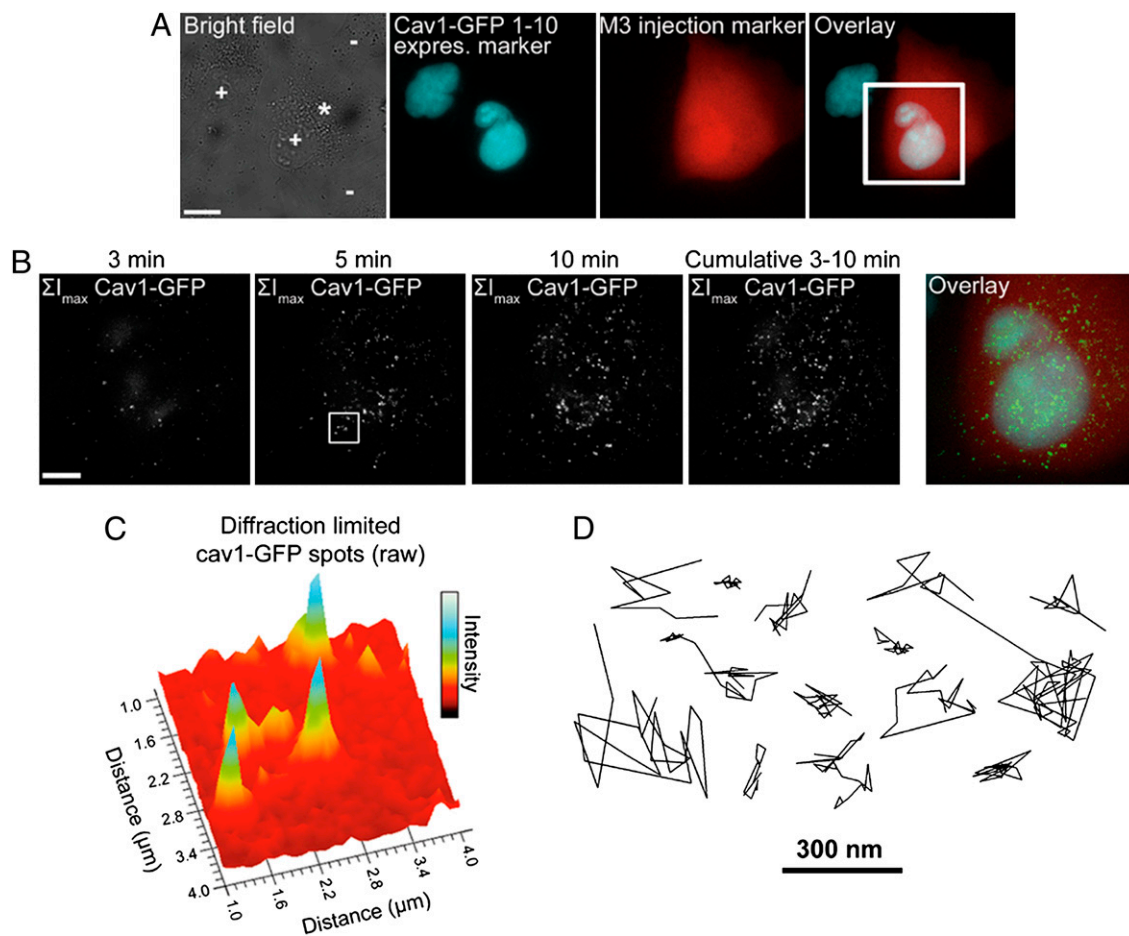
Fig. 3. SM imaging and tracking of extracellular GFP 1–10-CD4 proteins by CALM. (*A*) A region of interest (black square) in the plasma membrane of a U2OS cell stably expressing GFP 1–10-CD4 is imaged by TIRF before and after complementation with biotin-M3 peptides at different incubation times. Diffraction-limited single GFP-CD4 spots appear and diffuse in the plasma membrane within minutes of M3 peptide addition. Single GFP-CD4 spots are intentionally expanded to facilitate visualization. (Scale bar: 5 μm.) (*B*) Pixel-based maximum intensity projections (ΣI_{max}) TIRF images of all complemented GFP-CD4 detected during 20-min complementation with 1.8 or 18 μM biotin-M3 peptides (Movie S6). The field of view corresponds to the bright field image in *A*. (Scale bar: 5 μm.) (*C*) 3D rendering of raw and Gaussian-fitted diffraction-limited spots corresponding to individual complemented GFP-CD4 in the cell plasma membrane (white square in *A*). (*D*) Representative trajectories from single GFP-CD4 diffusing in the plasma membrane of U2OS cells during CALM imaging.

cross-correlation spectroscopy (FCCS) measurements all indicated that functionalized M3 peptides were irreversibly bound to complemented GFPs. This irreversible binding, consistent with prior reports on this split-GFP (11) and most BiFc systems (9), provided a means to use GFP 1–10 as a targeting platform. Thus, we used functionalized synthetic M3 peptides as vehicles for site-directed posttranslational modification of split-GFP fusion proteins in living cells, using GFP fluorescence as an effective signal of the targeting specificity (Fig. 5*A*). Cells expressing GFP 1–10-CD4 proteins were efficiently complemented by M3-A647 peptide conjugates, and GFP fluorescence was specifically activated at the plasma membrane, which was colabeled with M3-A647 (Fig. 5*B*). Relying on the absence of colocalizing GFP signal, we could also easily identify a few intracellular vesicles containing endocytosed and noncomplemented M3-A647 peptides observed in the Alexa 647 channel for both expressing and nonexpressing cells. The 1:1 stochiometry complementation of GFP 1–10-CD4 by M3-A647 was clearly observed by dual-color TIRF imaging. At the plasma membrane, single complemented A647-GFP-CD4 proteins emitted in both detection channels and diffused as individual colocalizing spots in a correlated manner before photobleaching in a single step (Fig. 5*C* and Movies S9 and S10). The presence of a few noncolocalizing GFP and M3-A647 molecules was due to incidental photobleaching of one of two probes in A647-GFP-CD4 proteins during imaging or to rare nonspecific membrane binding of M3-A647 peptides. Using the complementation-induced coincident SM detection of both probes as a selection criterion, we could focus our analysis only on specifically targeted M3-A647 peptides, rejecting fluorophores nonspecifically bound to the plasma membrane. A second advantage of this dual detection scheme was that single proteins could be tracked with brighter fluorophores and for longer times than afforded by the complemented GFP alone. For instance, tracking M3-A647 sometimes allowed for a doubling of the tracking time, even after photobleaching of GFP in A647-GFP-CD4 proteins (Fig. 5*C*).

Minutes-long tracking of single split-GFP fusion proteins was also achieved by complementation-induced targeting of highly photostable qdot probes. M3-qdots were produced by coating hydrophobic CdSe/ZnS qdots (545 nm emission, ~4 nm core/shell diameter) with synthetic peptides containing the C-terminal M3 sequence and an N-terminal semiconductor binding domain (25, 26) (FCC-M3). These compact peptide-coated M3-qdots (~10 nm diameter) specifically labeled cells expressing the transmembrane GFP 1–10-CD4 fusion proteins (Fig. 5*D*), and complemented qdot-GFP-CD4 could be tracked for extended periods (Fig. 5*E* and Movie S11). Despite their size and the reduced conformational freedom of surface-attached M3 peptides, small M3-qdots could efficiently target split-GFP fusion proteins in living cells, and diffusing qdots were easily identified on labeled cells (Movie S11). The presence of a few qdots bound to

Fig. 4. SM imaging and tracking of intracellular cav1-GFP 1–10$_{(h)}$ proteins by CALM. (*A*) A U2OS cell coexpressing cav1-GFP 1–10$_{(h)}$ and the nucleus-localized CFP-LacI-NLS coexpression marker (+) are microinjected with biotin-M3 peptides (∼5 μM final intracellular concentration) together with a biotin-Alexa 647 injection marker (star). A region of interest (white square) is then imaged for GFP fluorescence by TIRF microscopy. (Scale bar: 10 μm.) (*B*) Pixel-based maximum intensity projection (ΣI_{max}) TIRF images of all complemented cav1-GFP$_{(h)}$ detected at the ventral intracellular plasma membrane for the region of interest in *A* 3, 5, and 10 min after injection of M3 peptides (Movie S8). When overlaid with the wide-field fluorescence image, the cumulative 3- to 10-min maximum intensity projection image shows the high specificity of complementation. (Scale bar: 5 μm.) (*C*) 3D rendering of raw diffraction-limited spots corresponding to membrane-associated single cav1-GFP$_{(h)}$ proteins (white square in *B*). (*D*) Representative trajectories from single cav1-GFP$_{(h)}$ diffusing in the cytoplasmic side of the plasma membrane of U2OS cells during CALM imaging.

the fibronectin-coated coverslips or nonexpressing cells was due to the 1-h-long incubation time. The complementation efficacy was, however, significantly reduced for CdSe/ZnS qdots with core/shell sizes above ∼4–5 nm, suggesting that M3 peptide accessibility and flexibility need to be further optimized for larger qdots. Although the insufficient spectral separation between qdots and GFP in complemented qdot-GFP-CD4 prevented SM coincident imaging in cells, coincident detection of one or multiple copies of complemented GFP-biotin bound to individual red-emitting streptavidin-coated qdots was achieved by in vitro TIRF imaging (*SI Appendix*, Fig. S10).

Single Biomolecule Tracking by Complementation-Induced Intramolecular spFRET in Living Cells. An additional imaging modality afforded by CALM involved intramolecular spFRET between a complemented split-GFP fusion protein and an acceptor fluorophore attached to an M3 peptide. Although we intentionally chose the red-shifted Alexa 647 dye to limit spectral overlap between complemented GFPs and M3-A647 conjugates (*SI Appendix*, Fig. S11), significant FRET from A647-GFP complexes was observed in native gels (Fig. 6*A* and *SI Appendix*, Fig. S11). The mean FRET efficiency in solution, determined from changes in GFP fluorescence lifetime was E ∼ 0.3, indicating that the

M3-attached Alexa 647 fluorophore is less than 4 nm away from the GFP chromophore after complementation. In living cells, intramolecular spFRET was confirmed by detecting Alexa 647 fluorescence at the plasma membrane of U2OS using 488-nm TIRF excitation of GFP 1–10-CD4 fusion proteins complemented with M3-A647 peptides (Fig. 6*B* and Movie S12). Under the same 488-nm excitation, cells complemented with nonfluorescent M3-biotin showed no FRET but an expected brighter GFP signal. Single complemented A647-GFP-CD4 proteins were identified as diffusing colocalized spots that emitted in both detection channels (Movie S13), and direct evidence for spFRET was obtained by plotting GFP-CD4 and M3-A647 fluorescence intensity time traces along the diffusion path of individual A647-GFP-CD4 proteins (Fig. 6*C*). Consistent with intramolecular spFRET, FRET signal was altogether lost on single-step GFP photobleaching (Fig. 6*C*). When M3-A647 photobleached before GFP-CD4, a large anticorrelated increase in GFP intensity was immediately observed (Fig. 6*C*).

By combining CALM and indirect spFRET excitation of M3-A647, we could specifically label and track CD4 proteins in living cells using very high fluorophore concentrations and no washing. Indeed, the large-excitation Stoke shift (>150 nm) afforded by 488-nm spFRET excitation prevented the excitation of non-
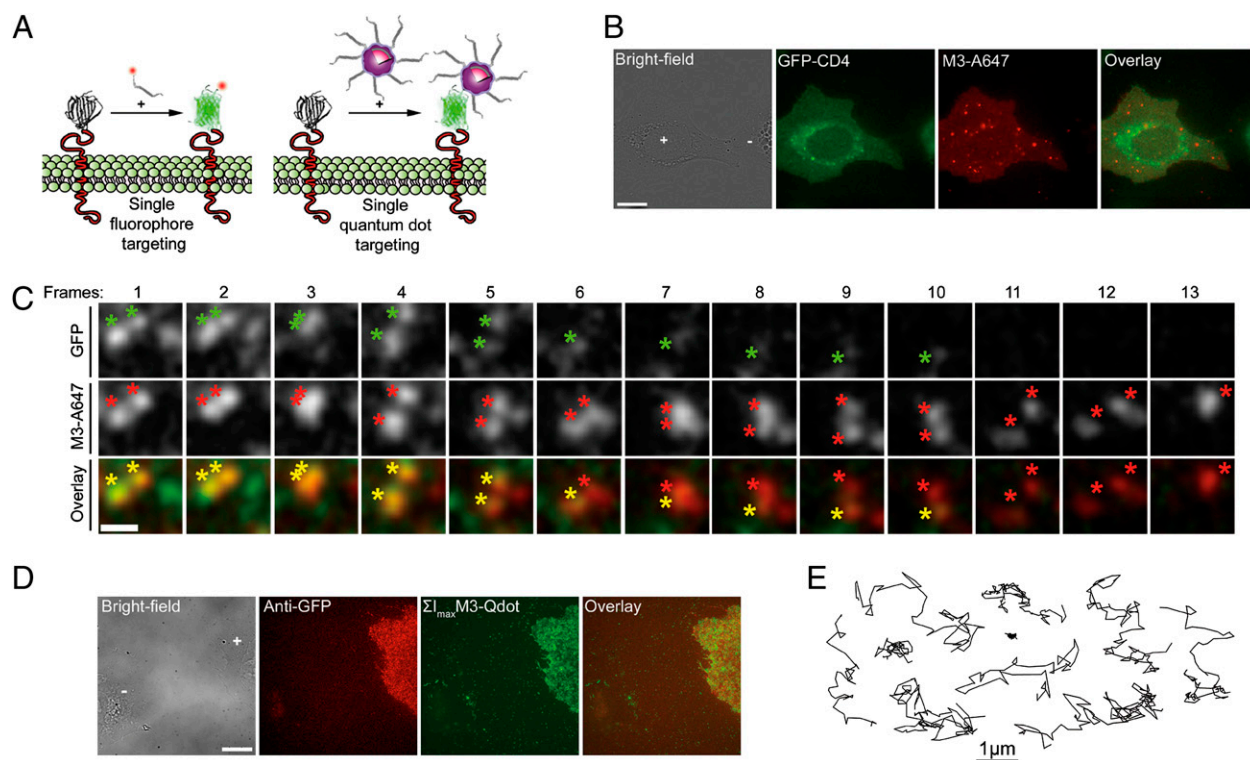
Fig. 5. Addressable live cell targeting and tracking of single fluorophores and qdots by CALM. (*A*) Schematic of CALM with fluorescent M3 peptide conjugates and M3 peptide-coated qdots. (*B*) Labeling of a GFP 1–10-CD4–expressing U2OS cells (+) with M3-A647 peptide conjugates. (Scale bar: 10 μm.) (*C*) Coincident dual-color detection of single diffusing A647-GFP-CD4 proteins by TIRF in U2OS cells. Colocalizing diffraction-limited spots are simultaneously detected in the GFP and M3-A647 channels (colored asterisks). During diffusion, GFP photobleaches in a single step (frames 6 and 11), but A647-GFP-CD4 proteins can still be tracked in the M3-A647 channel before disappearing on M3-A647 photobleaching (frame 13). The diffraction-limited spots are intentionally expanded to facilitate visualization (Movie S10). (Scale bar: 1 μm.) (*D*) Wide-field fluorescence imaging of peptide-coated CdSe/ZnS M3-qdots specifically targeted to U2OS cells expressing GFP 1–10-CD4 fusion proteins (+). The M3-qdot image is a pixel-based maximum intensity projection of diffusing M3-qdots (ΣI_{max}) for all frames of Movie S11. (Scale bar: 15 μm.) (*E*) Representative trajectories from qdot tracking of single complemented qdot-GFP-CD4 proteins diffusing in the plasma membrane of U2OS cells.

bound M3-A647, which remained dark when excited by TIRF despite concentrations of ~1 μM in the imaging buffer of GFP 1–10-CD4–expressing cells. When complemented A647-GFP-CD4 proteins were directly excited at 638 nm, the elevated M3-A647 concentration in the buffer prevented the detection of individual proteins (Fig. 6*D*). However, on 488-nm excitation, individual A647-GFP-CD4 proteins were specifically detected in both the GFP and Alexa 647 channels, with no interference from excess nonbound M3-A647 peptides (Fig. 6*D* and Movie S14). In the Alexa 647 channel, diffusing A647-GFP-CD4 proteins undergoing spFRET could easily be tracked, despite M3-A647 concentration orders of magnitude higher than normally required for SM imaging.

Discussion

CALM is a versatile approach for very high confidence targeting and imaging of single biomolecules in living cells. Its use of an asymmetric split-GFP is advantageous, because one of the fragments can be produced synthetically with great flexibility for advanced designs. The ability to reconstruct and activate dark split-GFPs fusion proteins into bright GFPs by simple external addition of self-complementary synthetic peptides provides a flexible means for low-background and ultra-specific imaging of a controlled subset of biomolecules, even when they are highly expressed. Indeed, in CALM, both the stochastic binding of M3 peptides and the chromophore maturation time, which drive GFP appearance, are key to spreading protein activation in time and space and to facilitating low-density tracking. Thus, by simply

adjusting the concentration of complementary peptides and incubation times, hundreds to thousands of individual biomolecules can be continuously recorded, or the entire population can be imaged.

As shown for three different proteins in a variety of cell lines, CALM imaging requires a simple GFP 1–10 fusion and relatively inexpensive synthetic peptides. The proper organelle association and diffusive behaviors of the N- and C-terminal split-GFP fusion proteins that we have tested indicate that CALM should easily apply to other extra- and intracellular proteins. CALM is, in principle, simpler than cell-labeling techniques such as Bir-A ligase (27), PRIME (28), ACP-tag (29), or Sortase (30), which necessitate enzyme-assisted ligation. An additional advantage of CALM over these techniques and other labeling methods (31–34) is that no washing of excess probes is necessary, because fluorescence is only generated on GFP complementation and specific detection of only the targeted proteins can be achieved by CALM-spFRET. In this respect, CALM resembles the recently introduced fluorogen-activating single-chain antibodies (35), with the important advantages that our approach allows irreversible linkage, does not require extensive protein or probe engineering for multiplexing, enables SM imaging, and works efficiently inside living cells, where the reducing cytoplasmic environment might interfere with the activity of some single-chain antibodies (35).

Compared with tracking with photoswitchable or photoactivable FPs (6, 36) (sptPALM), where a large number of SMs can be imaged in live cells immediately after laser activation, the complementation kinetics of our current split-GFP can generate

Fig. 6. Cell imaging and single biomolecule tracking by complementation-induced intramolecular spFRET. (*A*) In vitro native gel shift assay of M3-A647 peptide binding to soluble GFP 1–10 (+) or in TGN buffer (−). The gel is sequentially imaged for M3-A647, GFP, and A647-GFP intramolecular FRET emission. (*B*) Live cell imaging of GFP 1–10-CD4 proteins complemented with fluorescent M3-A647 (*Left*) or nonfluorescent M3-biotin (*Right*) peptides and imaged by dual-color TIRF microscopy using only 488-nm excitation. Images are pixel-based maximum intensity projections of diffusing A647-GFP-CD4 proteins (ΣI_{max}) for all frames of Movie S12. (Scale bar: 5 μm.) (*C*) GFP (green) and M3-A647 fluorescence time traces (red) along the diffusion path (*Right*) of individual A647-GFP-CD4 proteins showing intramolecular spFRET. Fluorescence background traces (gray) are taken in the immediate vicinity of the trajectories. The single-step photobleaching of GFP (*Upper*, green arrow) or M3-A647 (*Lower*, red arrow) induces an arrest of intramolecular spFRET (Movie S13). (*D*) Live cell TIRF imaging and tracking of individual A647-GFP-CD4 proteins by spFRET at high M3-A647 concentrations (0.7 μM) without washing. A cell is sequentially imaged using direct M3-A647 excitation at 638 nm (*Left*) and then, indirect spFRET excitation at 488-nm laser (*Right*). Individual A647-GFP-CD4 proteins diffusing in the plasma membrane can be tracked in the M3-A647 channel using indirect spFRET excitation (red trajectories and white squares) but are lost in the saturating surrounding fluorescent signal when directly excited at 638 nm (red squares). Three representative examples of A647-GFP-CD4 trajectories are presented (from white squares). (Scale bar: 10 μm.)

a short delay (∼2–3 min) between the addition of complementary peptides and the detection of statistically significant SM events during CALM imaging. However, at longer incubation times and appropriate peptide concentrations, the average SM activation and tracking density are similar to those of sptPALM. In addition, CALM has a few advantages over sptPALM. For instance, it does not require additional lasers other than the imaging 488-nm laser for SM detection, which simplifies optical setups. Importantly, split-GFP fusion proteins are dark and do not undergo self-activation, even at elevated protein expression, which is contrary to some photoswitchable FPs (37). Finally, the sto-

chastic binding of peptides and maturation time in CALM make it unlikely that multiple split-GFP fusion proteins packed in a subcellular structure be simultaneous activated. Thus, CALM might offer a favorable alternative to sptPALM for live imaging of single biomolecules associated with highly crowded cellular nanostructures, which is shown by our ability to track individual cav1-GFP$_{(h)}$ within 50- to 100-nm caveolae containing ∼150 copies of cav1 (38). Current limitations of CALM include the need for peptide carriers (*SI Appendix*, Fig. S8) or microinjection for intracellular delivery and imaging and limited spatial control of the activation compared with sptPALM. Some of these issues

might be solved by advanced engineering of complementary synthetic peptides.

An important specificity of CALM is that individual proteins are not only detected and imaged with nanometer precision but are also irreversibly modified, posttranslationally, within living cells. Engineered complementary peptides can, thus, be used as vectors for site-directed and stochiometric targeting of exogenous chemical moieties and probes to proteins of interest in living cells, as shown here with M3-biotin, M3-A647, and M3-qdots. With CALM, the built-in feedback on targeting efficiency provided by the appearance of GFP allows for a minimization of analytical artifacts related to nonspecific binding of probes, which is often unpredictable at the SM level in cells. Using co-incident SM detection, mislocalized probes can be filtered out of the analysis or altogether ignored if imaging is performed by CALM-spFRET. Although we showed CALM-spFRET for external proteins only, this approach should greatly simplify SM imaging inside living cells and in living animals. Indeed, by allowing specific tracking of single biomolecules independently of their expression level and at very high probe concentrations, CALM-spFRET alleviates issues associated with inappropriate protein expression levels or inadequate intracellular or intravital probe delivery.

As for all imaging methodologies that use FPs, SM tracking by CALM or CALM-spFRET is limited by the photostability of GFP. However, as we have shown, longer tracking can be achieved using CALM-targeted fluorophores or qdots. CALM should be easily extended to other photostable SM probes like quantum rods, nanodiamonds, or fluorescent beads functionalized with M3 peptides, and it will be useful for light-assisted targeting of other nanomaterials. For these nanomaterials, including qdots, CALM readily solves the complicated issues of surface mono-functionalization (39, 40). Indeed, as we have shown, counting complemented GFPs on a single probe provides a direct readout of its valency and can be used as a criterion to filter out cross-linked probes from the analysis or correlate the diffusive behavior of a protein with its clustering state.

Here we have used CALM with split-GFP only, but the technique is, in principal, extendable to other variants such as split-CFP or split-YFP, which are also derived from *Aequorea Victoria* GFP. These variants should facilitate multicolor SM imaging in living cells using a unique M3 complementary synthetic peptide common to all these split-FPs. Additional developments of red-shifted split-FPs will also broaden the panel of genetically encoded probes for CALM. Sets of split-FPs, sets of complementary M3 peptide fluorophore conjugates, and sets of M3-qdots will constitute a modular toolkit for easy tailoring of SM probes to specific biological applications in vitro, in cells, and in vivo.

In conclusion, CALM uniquely combines targeting, imaging, and addressable posttranslational synthetic modification of biomolecules in living cells with SM sensitivity and nanometer precision. In addition to allowing ever more controlled SM imaging in complex biological environments, CALM also provides new bioimaging and manipulation modalities for cellular biology.

Methods

Design of Synthetic Split-GFP M3 Complementation Fragments.
Complementary peptides to GFP 1–10 and GFP 1–10 fusion proteins were designed based on the GFP 11 M3 sequence published by Cabantous et al. (10). All synthetic peptides were obtained at >70% or >95% purity (Biomatik or New England Peptide), and their identity and purity were confirmed by MS. A biotinylated M3 peptide (biotin-M3) was designed with an N-terminal biotin, an amidocaproyl (acp) linker, a short 8-aa linker, and the C-terminal M3 amino acid sequence (underlined) biotin-acp-GSGGGGSTS<u>RDHMVLHEYVNAAGIT</u> (MW = 2,756 Da). A cysteine-terminated M3 peptide (Cys-M3) was used for conjugation to fluorophores such as Alexa Fluor 647 C_2 maleimide (Invitrogen). Cys-M3 contains an N-terminal cysteine residue, an acp linker, a short 8-aa peptide linker, and the C-terminal M3 sequence (underlined) C-acp-

GSGGGGSTS<u>RDHMVLHEYVNAAGIT</u> (MW = 2,633 Da). For the functionalization of qdots with M3 peptides, we designed a synthetic peptide based on engineered cysteine-rich peptides capable of specifically binding on the semiconductor surface of CdSe/ZnS qdots (25, 26). This peptide (FCC-M3) contains an acetylated N terminus, an N-terminal qdot binding domain (in bold), a flexible and pegylated amino acid linker, and the C-terminal M3 sequence (underlined) $_{ac}$-**FCCFCCFCCF**GGSESG-peg$_6$-GSGGGGSTS<u>RDHMVL-HEYVNAAGIT</u> (MW = 4,476 Da).

Cell Transfection, Staining, and Imaging.
All cell lines (U20S, HEK, and COS-7) were cultured in DMEM + 10% fetal calf serum (FCS) at 37 °C in 5% CO_2. Transient and stable transfections with GFP 1–10-CD4, GFP 1–10$_{(h)}$-GPI, and cav1-GFP 1–10$_{(h)}$ expression vectors were performed with lipofectamine (Invitrogen) or fugene (Roche) reagents. To visualize cells expressing cav1-GFP 1–10$_{(h)}$ before microinjections of the complementary M3 peptides, the cav1-GFP 1–10$_{(h)}$-N1 expression plasmid was transiently cotransfected with either a plasmid encoding the nuclear CFP-LacI-NLS or a plasmid encoding the actin-binding peptide mCherry-LifeAct. No cotransfection was performed for immunolabeling of cav1-GFP 1–10$_{(h)}$–expressing cells. Detailed experimental protocols for ensemble and SM extracellular and intracellular staining with biotin-M3, Cys-M3, FCC-M3, and M3-A647 peptides, M3-qdots, Alexa-647–labeled anti-GFP, and Alexa-647–labeled streptavidin are available in *SI Appendix, SI Methods*. Cells grown on fibronectin-coated glass coverslips to 70–80% confluency were imaged in Tyrode's (136 mM NaCl, 10 mM KCl, 0.4 mM $MgCl_2$, 1.0 mM $CaCl_2$, 5.6 mM Glucose, 10.0 mM Hepes, pH 7.8) or Hepes-buffered HBSS (145 mM NaCl, 5 mM KCl, 1.2 mM $MgSO_4$, 2.0 mM $CaCl_2$, 1.2 mM NaH_2PO_4, 10 mM glucose, 20.0 mM Hepes, pH 7.6) at 37 °C.

Optical Setups.
Wide-field epifluorescence imaging was performed on an IX70 Olympus inverted microscope equipped with a ×100, 1.45 NA objective, a UV lamp, and appropriate optical filters for imaging CFP, GFP, mCherry, or Alexa Fluor 647. Fluorescence was detected on a QuantEM:512SC EMCCD camera (Photometrics). TIRF imaging was performed on the same microscope using a custom-built optical setup allowing simultaneous dual-color laser excitation at 488 and 638 nm and simultaneous dual-color detection through a DV2 Dual-View system (Photometrics) equipped with appropriate filters and mirrors for the detection of GFP and Alexa 647 on the EMCCD camera. Coincidence SM imaging and FRET imaging of A647-GFP-CD4 complexes in cells were performed by TIRF using simultaneous dual excitation at 488 and 638 nm or single excitation at 488 nm, respectively, and dual-color detection, respectively.

Tracking and Diffusion Analysis of Single Split-GFPs, Single Fluorophores, and Single Qdots in Living Cells.
All SM tracking and subsequent analyses were done using a series of homemade software called AsteriX and written in Labview (22). Tracking was done by 2D Gaussian fitting of individual diffraction-limited spots corresponding to single complemented split-GFPs, single fluorophores, or single qdots in each frame of the acquired videos. Single trajectories are represented by the fitted positions connected by a straight line. The mean trajectory lengths are reported in seconds ± SD of the mean (*SI Appendix*, Table S1). The localization uncertainty for single proteins was estimated as previously described (41–43) and is reported as a mean value in nanometer ± SD of the mean (*SI Appendix, SI Methods* and Table S1). The software also makes possible the exporting of a diffusion trajectory tracked in one channel (e.g., GFP channel) to a second channel (e.g., Alexa 647 channel) acquired simultaneously. After image correction and alignment, it is possible to obtain M3-A647 intensity–time traces along the diffusion path of a complemented GFP 1–10 fusion protein. Using this approach, single-pair FRET signals from diffusing A647-GFP-CD4 proteins were obtained by correlating fluorescence intensity time traces from both Alexa 647 and GFP channels along the diffusion trajectory of single proteins.

Diffusion analyses were performed as previously described (22) on ensemble MSD curves (*SI Appendix*, Fig. S6) and ensemble histograms of probability distribution of the square displacements (P_r^2) (19). Diffusion coefficients were obtained by fitting the MSD and P_r^2 curves on the first four nonzero points of the curves (D_1–D_4) using a simple Brownian diffusion model with measurement error: $4\sigma^2 + 4Dt$. Diffusion coefficients are reported in micrometers squared per second ± SD of the fit. Analyses by P_r^2 also provide an additional set of parameters (α_i), which indicates the fraction of each subpopulation detected. These fractions are reported in percentages (*SI Appendix*, Table S1).

Additional information on biochemical, analytical, and synthetic methods, in vitro complementation assays, cloning, cell labeling and imaging, optical setups, and other protocols is in *SI Appendix, SI Methods*.

1. Lord SJ, Lee HLD, Moerner WE (2010) Single-molecule spectroscopy and imaging of biomolecules in living cells. *Anal Chem* 82:2192–2203.
2. Pinaud F, Clarke S, Sittner A, Dahan M (2010) Probing cellular events, one quantum dot at a time. *Nat Methods* 7:275–285.
3. Yano Y, Matsuzaki K (2009) Tag-probe labeling methods for live-cell imaging of membrane proteins. *Biochim Biophys Acta* 1788:2124–2131.
4. Giepmans BNG, Adams SR, Ellisman MH, Tsien RY (2006) The fluorescent toolbox for assessing protein location and function. *Science* 312:217–224.
5. Shroff H, Galbraith CG, Galbraith JA, Betzig E (2008) Live-cell photoactivated localization microscopy of nanoscale adhesion dynamics. *Nat Methods* 5:417–423.
6. Hess ST, et al. (2007) Dynamic clustered distribution of hemagglutinin resolved at 40 nm in living cell membranes discriminates between raft theories. *Proc Natl Acad Sci USA* 104:17370–17375.
7. Heilemann M, van de Linde S, Mukherjee A, Sauer M (2009) Super-resolution imaging with small organic fluorophores. *Angew Chem Int Ed Engl* 48:6903–6908.
8. Lippincott-Schwartz J, Patterson GH (2009) Photoactivatable fluorescent proteins for diffraction-limited and super-resolution imaging. *Trends Cell Biol* 19:555–565.
9. Kerppola TK (2008) Bimolecular fluorescence complementation (BiFC) analysis as a probe of protein interactions in living cells. *Annu Rev Biophys* 37:465–487.
10. Cabantous S, Terwilliger TC, Waldo GS (2005) Protein tagging and detection with engineered self-assembling fragments of green fluorescent protein. *Nat Biotechnol* 23:102–107.
11. Cabantous S, Waldo GS (2006) In vivo and in vitro protein solubility assays using split GFP. *Nat Methods* 3:845–854.
12. Sakamoto S, Kudo K (2008) Supramolecular control of split-GFP reassembly by conjugation of beta-cyclodextrin and coumarin units. *J Am Chem Soc* 130:9574–9582.
13. Kent KP, Childs W, Boxer SG (2008) Deconstructing green fluorescent protein. *J Am Chem Soc* 130:9664–9665.
14. Feinberg EH, et al. (2008) GFP Reconstitution Across Synaptic Partners (GRASP) defines cell contacts and synapses in living nervous systems. *Neuron* 57:353–363.
15. Van Engelenburg SB, Palmer AE (2010) Imaging type-III secretion reveals dynamics and spatial segregation of Salmonella effectors. *Nat Methods* 7:325–330.
16. Rothberg KG, et al. (1992) Caveolin, a protein component of caveolae membrane coats. *Cell* 68:673–682.
17. Hailstones D, Sleer LS, Parton RG, Stanley KK (1998) Regulation of caveolin and caveolae by cholesterol in MDCK cells. *J Lipid Res* 39:369–379.
18. Bush WS, Ihrke G, Robinson JM, Kenworthy AK (2006) Antibody-specific detection of caveolin-1 in subapical compartments of MDCK cells. *Histochem Cell Biol* 126:27–34.
19. Schütz GJ, Schindler H, Schmidt T (1997) Single-molecule microscopy on model membranes reveals anomalous diffusion. *Biophys J* 73:1073–1080.
20. Fragoso R, et al. (2003) Lipid raft distribution of CD4 depends on its palmitoylation and association with Lck, and evidence for CD4-induced lipid raft aggregation as an additional mechanism to enhance CD3 signaling. *J Immunol* 170:913–921.
21. Popik W, Alce TM (2004) CD4 receptor localized to non-raft membrane microdomains supports HIV-1 entry. Identification of a novel raft localization marker in CD4. *J Biol Chem* 279:704–712.
22. Pinaud F, et al. (2009) Dynamic partitioning of a glycosyl-phosphatidylinositol-anchored protein in glycosphingolipid-rich microdomains imaged by single-quantum dot tracking. *Traffic* 10:691–712.
23. Morris MC, Depollier J, Mery J, Heitz F, Divita G (2001) A peptide carrier for the delivery of biologically active proteins into mammalian cells. *Nat Biotechnol* 19:1173–1176.
24. Thomsen P, Roepstorff K, Stahlhut M, van Deurs B (2002) Caveolae are highly immobile plasma membrane microdomains, which are not involved in constitutive endocytic trafficking. *Mol Biol Cell* 13:238–250.
25. Pinaud F, King D, Moore HP, Weiss S (2004) Bioactivation and cell targeting of semiconductor CdSe/ZnS nanocrystals with phytochelatin-related peptides. *J Am Chem Soc* 126:6115–6123.
26. Iyer G, Pinaud F, Tsay J, Weiss S (2007) Solubilization of quantum dots with a recombinant peptide from Escherichia coli. *Small* 3:793–798.
27. Chen I, Howarth M, Lin WY, Ting AY (2005) Site-specific labeling of cell surface proteins with biophysical probes using biotin ligase. *Nat Methods* 2:99–104.
28. Uttamapinant C, et al. (2010) A fluorophore ligase for site-specific protein labeling inside living cells. *Proc Natl Acad Sci USA* 107:10914–10919.
29. George N, Pick H, Vogel H, Johnsson N, Johnsson K (2004) Specific labeling of cell surface proteins with chemically diverse compounds. *J Am Chem Soc* 126:8896–8897.
30. Tanaka T, Yamamoto T, Tsukiji S, Nagamune T (2008) Site-specific protein modification on living cells catalyzed by Sortase. *ChemBioChem* 9:802–807.
31. Martin BR, Giepmans BNG, Adams SR, Tsien RY (2005) Mammalian cell-based optimization of the biarsenical-binding tetracysteine motif for improved fluorescence and affinity. *Nat Biotechnol* 23:1308–1314.
32. Lata S, Gavutis M, Tampé R, Piehler J (2006) Specific and stable fluorescence labeling of histidine-tagged proteins for dissecting multi-protein complex formation. *J Am Chem Soc* 128:2365–2372.
33. Keppler A, et al. (2003) A general method for the covalent labeling of fusion proteins with small molecules in vivo. *Nat Biotechnol* 21:86–89.
34. Los GV, et al. (2008) HaloTag: A novel protein labeling technology for cell imaging and protein analysis. *ACS Chem Biol* 3:373–382.
35. Szent-Gyorgyi C, et al. (2008) Fluorogen-activating single-chain antibodies for imaging cell surface proteins. *Nat Biotechnol* 26:235–240.
36. Manley S, et al. (2008) High-density mapping of single-molecule trajectories with photoactivated localization microscopy. *Nat Methods* 5:155–157.
37. Nowotschin S, Hadjantonakis AK (2009) Use of KikGR a photoconvertible green-to-red fluorescent protein for cell labeling and lineage analysis in ES cells and mouse embryos. *BMC Dev Biol* 9:49–61.
38. Lajoie P, Goetz JG, Dennis JW, Nabi IR (2009) Lattices, rafts, and scaffolds: Domain regulation of receptor signaling at the plasma membrane. *J Cell Biol* 185:381–385.
39. Clarke S, et al. (2010) Covalent monofunctionalization of peptide-coated quantum dots for single-molecule assays. *Nano Lett* 10:2147–2154.
40. Howarth M, et al. (2008) Monovalent, reduced-size quantum dots for imaging receptors on living cells. *Nat Methods* 5:397–399.
41. Michalet X (2010) Mean square displacement analysis of single-particle trajectories with localization error: Brownian motion in an isotropic medium. *Phys Rev E Stat Nonlin Soft Matter Phys* 82:041914-1–041914-13.
42. Michalet X, Lacoste TD, Weiss S (2001) Ultrahigh-resolution colocalization of spectrally separable point-like fluorescent probes. *Methods* 25:87–102.
43. Thompson RE, Larson DR, Webb WW (2002) Precise nanometer localization analysis for individual fluorescent probes. *Biophys J* 82:2775–2783.

Supporting Information

Pinaud and Dahan 10.1073/pnas.1101929108

**Supporting Information Corrected June 29, 2011**
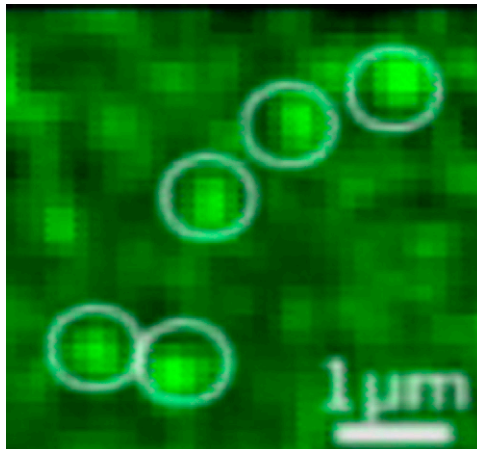
Movie S1. Single-molecule (SM) imaging of complemented split-GFP in vitro. GFP 1–10 are complemented in vitro with synthetic biotin-M3 peptides and deposited on a clean glass coverslip. On single-step photobleaching, the GFPs sequentially disappear from the imaging field. Imaging is performed by TIRF with a 60 ms/frame integration. Video playback = 30 frames/s.
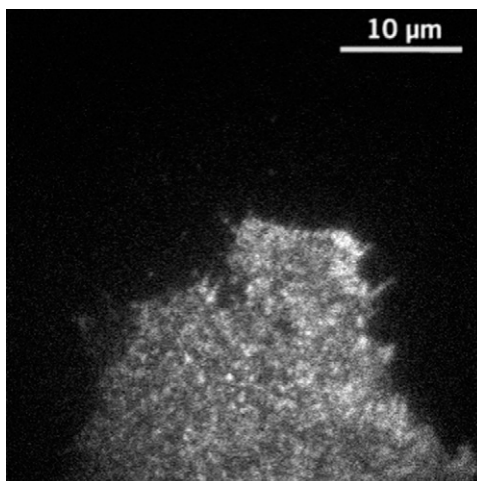
[Movie S1](#)

Movie S2. Total internal reflection fluorescence (TIRF) imaging of complemented GFP 1–10-CD4 proteins in the plasma membrane of U20S cells. Cells are incubated with 1.8 μM biotin-M3 for 45 min at 37 °C. The complementation is highly specific of the GFP 1–10-CD4–expressing cell, and individual GFP-CD4 proteins diffuse in the plasma membrane. Acquisition = 60 ms/frame. Video playback = 30 frames/s.

[Movie S2](#)
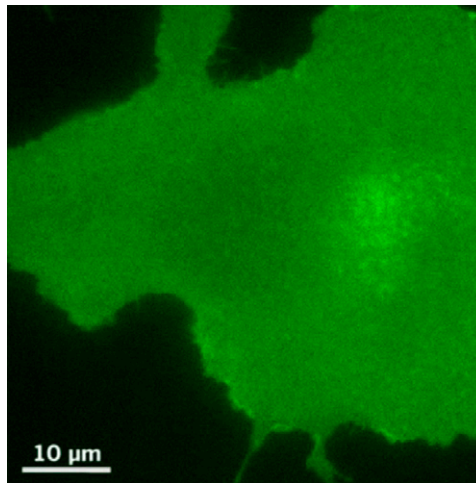
Movie S3. Wide-field fluorescence imaging of GFP 1–10$_{(h)}$-glycosylphosphatidyl inositol (GPI) proteins for long complementation times. GFP is imaged for a COS-7 cell expressing GFP 1–10$_{(h)}$-GPI and incubated at 37 °C for 48 h with 25 μM biotin-M3 complementary peptides in HBSS buffer + 20% FCS. Imaging frame rate = 60 ms/frame. Video playback = 30 frames/s.
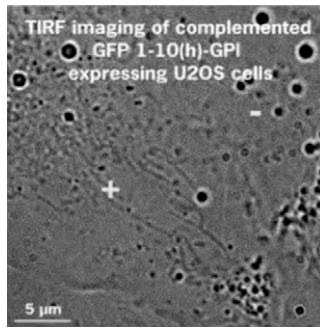
[Movie S3](#)
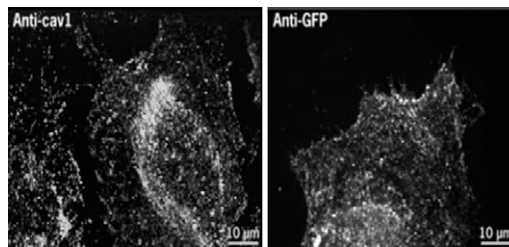
Movie S4. Immunostaining of endogenous caveolin-1 and caveolin-1–GFP 1–10 fusion proteins in U2OS cells. 3D projections of confocal sections for U2OS cells immunostained for endogenous caveolin-1 (anti-cav1; left) or GFP 1–10 after expression of cav1-GFP 1–10 (anti-GFP; right). In both cases, a typical punctuated pattern corresponding to caveolae-associated caveolin-1 is observed at the cell plasma membrane.

[Movie S4](#)

Movie S5. TIRF imaging of complemented intracellular caveolin-1–GFP 1–10 fusion proteins in living cells. Simultaneous dual-color TIRF imaging of U2OS cells coexpressing cav1-GFP 1–10$_{(h)}$ and actin-binding peptide (ABP)-mCherry after complementation by microinjection of synthetic M3 peptides (top) or no microinjection (bottom). The punctuated pattern of caveolae-associated and complemented cav1-GFP is visible at the ventral plasma membrane of the injected cell (zoom). Imaging is performed with a 100 ms/frame integration. Video playback = 30 frames/s. Note that the slight fluctuations at the beginning are because of a realignment of the TIRF excitation field.

[Movie S5](#)

Movie S6. Complementation-activated light microscopy (CALM) imaging of individual transmembrane GFP 1–10-CD4 in U2OS cells. The ventral plasma membrane of an expressing cell (top) and a nonexpressing cell (bottom) are repeatedly imaged every 5 min for about 1 min at a time before, during, and after addition of complementary M3 peptides at 1.8 μM imaging buffer. After 45 min of imaging, the same expressing cell (top) is imaged in the same manner after the addition of 18 μM complementary M3 peptides. The timing is provided in minute to second format and hour to minute to second format after 60 min. Imaging is performed with a 60 ms/frame integration. Video playback = 30 frames/s.

[Movie S6](#)

Movie S7. CALM imaging of individual lipid-anchored GFP 1–10(h)-GPI proteins in U2OS cells. The ventral plasma membranes of an expressing cell (+) and a nonexpressing cell (−) are imaged after 25 min incubation with 5 μM M3 complementary peptides at 37 °C. Notice the very high specificity of labeling for the expressing cell only. Imaging is performed with a 60 ms/frame integration. Video playback = 30 frames/s.

[Movie S7](#)
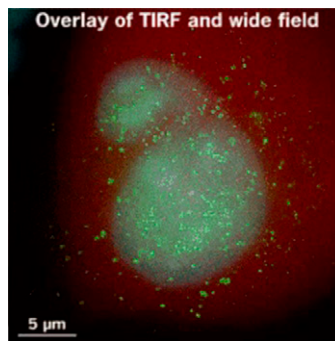
Movie S8. CALM imaging of individual intracellular cav-1–GFP(h) proteins in U2OS cells. The ventral plasma membranes of an expressing and microinjected cell (+ and *) and that of an expressing but not microinjected cell (+) are imaged at regular intervals (3, 5, and 10 min) for 30 s under continuous 488-nm laser excitation and after microinjection of M3 peptides. Notice the increasing amount of single cav1-GFP(h) lighting up at the membrane of the microinjected cell with increasing incubation times. Imaging is performed with a 100 ms/frame integration. Video playback = 30 frames/s.

[Movie S8](#)
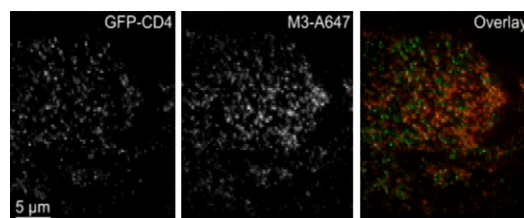
Movie S9. Simultaneous dual-color TIRF imaging of diffusing complemented A647-GFP-CD4 proteins in the plasma membrane of a U2OS cell. Imaging is performed by dual-color laser excitation at 488 and 638 nm and dual-color detection of A647-GFP-CD4 in separate GFP-CD4 and M3-A647 channels. Images from both channels have been overlaid after correction for alignment and chromatic aberrations (*SI Appendix, SI Methods*). Imaging is performed with a 100 ms/frame integration. Video playback = 10 frames/s.

[Movie S9](#)
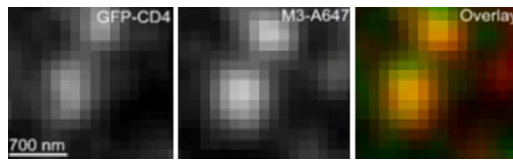
Movie S10. Coincident SM detection of complemented A647-GFP-CD4 proteins by dual-color TIRF imaging in U2OS cells. A region of interest from Movie S9 showing two diffusing A647-GFP-CD4 transmembrane proteins is selected. For both proteins, GFP photobleaches in a single step before the Alexa 647 fluorophore. The point spread functions of GFP-CD4 and M3-A647 have been intentionally expanded to facilitate visualization. Imaging is performed with a 100 ms/frame integration. Video playback = 10 frames/s.

Movie S10
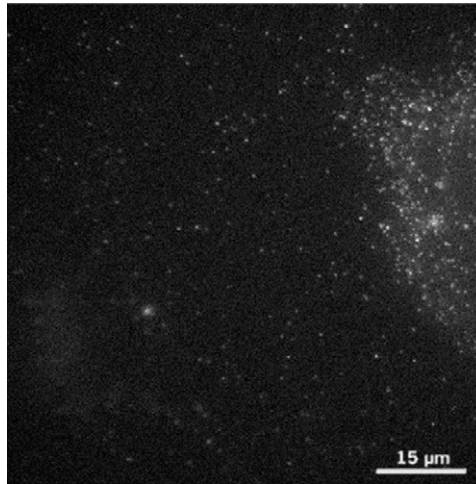
Movie S11. Wide-field fluorescence imaging of M3-quantum dots (qdots) targeted by CALM to GFP 1–10-CD4 proteins in U2OS cells. M3-qdots emitting at 545 nm specifically bind to the expressing cell (top right). The lateral membrane diffusion of single qdot-GFP-CD4 complexes at the cell surface and along filopodias is visible. Imaging is performed with a 100 ms/frame integration. Video playback = 30 frames/s.

Movie S11

Movie S12. Cell imaging by complementation-induced intramolecular single-pair Förster resonance energy transfer (spFRET). U2OS cells stably expressing the transmembrane GFP 1–10-CD4 fusion proteins are complemented with fluorescent M3-A647 (left) or nonfluorescent M3-biotin (right) peptides and imaged by dual-color TIRF microscopy using only a 488-nm laser excitation. spFRET from A647-GFP-CD4 proteins leads to fluorescence emission in the Alexa channel (left) but is absent from biotin-GFP CD4 proteins (right). Single A647-GFP-CD4 complexes can be seen diffusing in the membrane in both channels (left), with nonphotobleached complexes entering the TIRF field from the cell edge. Imaging is performed with a 60 ms/frame integration. Video playback = 30 frames/s.

Movie S12

Movie S13. Tracking individual proteins in living cells by intramolecular spFRET. Two regions of interest show individual complemented A647-GFP-CD4 proteins diffusing in the plasma membrane under continuous 488-nm laser excitation. The GFP and Alexa 647 channels have been overlaid to show that spFRET from single A647-GFP-CD4 proteins leads to fluorescence emission in both channels. In the left video, a diffusing A647-GFP-CD4 protein undergoes spFRET (yellow arrow) until GFP photobleaches in a single step, leading to disappearance of the protein. In the right video, another diffusing A647-GFP-CD4 protein undergoes spFRET (yellow arrow) until M3-A647 photobleaches in a single step. This leads to an arrest of spFRET and an increase in GFP fluorescence (green arrow) before the protein fully disappears on GFP single-step photobleaching. Imaging is performed with a 60 ms/frame integration. Video playback = 30 frames/s. Note that the left video is repeated three times.

Movie S13
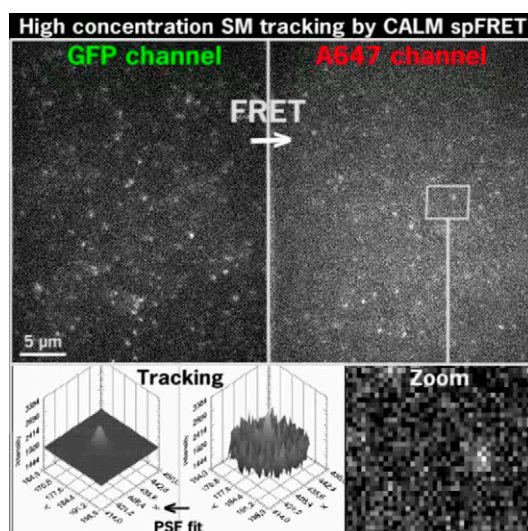
Movie S14. Live cell tracking of individual proteins at very high probe concentrations. A U2OS cell is incubated with 0.7 μM M3-A647 without washing and imaged by TIRF with a single laser excitation at 488 nm. Complemented A647-GFP-CD4 proteins are specifically excited at 488 nm and undergo spFRET, which is detected by the presence of diffusing and diffraction-limited fluorescence spots in the Alexa 647 channel. The lack of interference from the nonbound and large excess of M3-A647 peptides, which are not excited at 488 nm, together with the good spatial and temporal separation between complemented single A647-GFP-CD4 facilitate tracking in the Alexa 647 channel by 2D Gaussian fitting, despite the presence of ~1 μM fluorophore in the imaging media. Imaging is performed with a 60 ms/frame integration. Video playback = 10 frames/s.

Movie S14

Other Supporting Information Files

SI Appendix (PDF)

Targeting and imaging of single biomolecules in living cells by complementation activated light microscopy with split-fluorescent proteins

SUPPLEMENTARY INFORMATION

Fabien Pinaud[*] and Maxime Dahan

Laboratoire Kastler Brossel, Centre National de la Recherche Scientifique Unité de Recherche 8552, Physics Department and Institute of Biology, Ecole Normale Supérieure, Université Pierre et Marie Curie-Paris 6, 75005 Paris, France

* Laboratoire Kastler Brossel, Ecole Normale Supérieure, Institut de Biologie, 46 rue d'Ulm, 75005 Paris, France
Email: fabien.pinaud@lkb.ens.fr, Telephone: +33(0)1 44 32 33 92, Fax: +33(0)1 43 32 33 78.

Supplementary methods

In vitro **preparation of soluble GFP 1-10**. A pET GFP 1-10 plasmid encoding the GFP 1-10 was a kind gift of G. Waldo. Preparation of GFP 1-10 in *E.coli* BL21 (DE3) was done according to the protocol published by Cabantous et al. (1), with the exception that the bacterial supernatant containing the unpurified soluble fraction of GFP 1-10 (~50%) after sonication in 100 mM Tris/HCl, 150 mM NaCl, v/v 10% glycerol, pH 7.4 (TNG) buffer was kept and frozen at -80°C at a concentration of 0.5 mg/ml. Inclusion bodies and cell debris were discarded. In some *in vitro* complementation experiments, we intentionally choose to use non-purified GFP 1-10 in order to estimate the complementation efficiency between the two split-GFP fragments in protein-rich solutions that would reflect the environment encountered in living cells. Alternatively, purified GFP 1-10 was obtained in the form of the "Fold 'n' Glow" Split GFP Detection Reagent (Sandia Biotech).

Size exclusion High Pressure Liquid Chromatography (HPLC) analysis. Size exclusion HPLC was performed on a 1200 series LC system (Agilent) equipped with a Superdex^{TM} 200 column (GE Healthcare) or a TSK-GEL G4000SW (Tosoh Bioscience) using a PBS mobile phase (100 mM NaCl, 3 mM KCl, 2 mM KH_2PO_4, 7 mM Na_2HPO_4, pH 7.2) at a flow rate of 0.5 ml/min. Absorbance and fluorescence signals were acquired online, during the separation. Calibration of the columns was performed with a set of globular protein standards of known molecular weight (Biorad).

Conjugation of Alexa Fluor 647 C$_2$ maleimide to cysteine-M3 peptides and purification. A 15.0 mg/ml solution of Cys-M3 peptides was prepared by solubilizing 1.1 mg of lyophilized peptides in 10 µl DMSO (Sigma), and further diluting the solution with the addition of 65 µl of 0.1 M of triethylammonium acetate buffer (TEAA, Sigma). The peptide solution was then cleaned on a G-10 spin column (Harvard Apparatus) equilibrated with TN buffer (0.1 M Tris-HCl, 0.1 M NaCl and pH 6.8). A 1.1 fold molar excess of Alexa Fluor 647 C$_2$ maleimide (Invitrogen) at 5.5 mM in dimethylformamide was then incubated with the Cys-M3 peptide solution at room temperature for 3 hours with mixing every 30 minutes. Analysis of the M3-Alexa Fluor 647 peptide conjugate (M3-A647) and its purification were performed by reverse phase HPLC on a 1200 series LC system (Agilent) equipped with an Eclipse XDB-C18-Zorbax column (Agilent) and using an initial 0.1 M TEAA + 10% acetonitrile (ACN) mobile phase and a 30 minutes, linear 10 to 40 % ACN gradient (flow rate: 1.0 ml/min). Absorbance and fluorescence detections were performed online, during the separation. As seen in Figure S2, the M3-A647 peptide conjugate is well separated from the different components of the conjugation reaction under these chromatographic conditions. The conjugation efficiency was in the range of 40-30 %. The M3-A647 conjugate peak was collected, concentrated on a SpeedVac system and further cleaned on a G-10 spin column equilibrated with TN buffer + 10 % ACN. The purity of the M3-A647 peptide was >97% (Fig. S2), and the conjugate was stable and active for at least 1.5 months when conserved at 4°C. Assuming a 1:1 reaction stochiometry between a Cys-M3 peptide and an Alexa Fluor 647 maleimide fluorophore, the concentration of the purified M3-A647 conjugate was determined by absorption spectroscopy at 650 nm using an extinction coefficient ε_{650}= 239,000 cm^{-1}M^{-1} for Alexa Fluor 647 at the maximum absorption wavelength λ_{max}=650 nm.

Solubilization of quantum dots with FCC-M3 peptides and purification. Hydrophobic CdSe/ZnS quantum dots (qdots) (Invitrogen, Qdot 545 ITK organic) were coated with peptides using published procedures (2, 3). Briefly, 60 µl of the organic qdot solution at 1 µM were precipitated with a 3:1

methanol:isopropanol mixture, centrifuged, redisolved in 450 µl pyridine and gently refluxed for 1-2 minutes at high temperature to obtain a clear qdot solution in pyridine. A 50 µl DMSO solution containing a mixture of 40% FCC-M3, 30% ac-FCCFCCFCCF-PEG$_6$ and 30% ac-FCCFCCFCCFGSESGGSESGK peptides, totaling 4 mg, was then mixed with the qdot pyridine solution. The peptide coating was immediately triggered by the rapid addition of 11 µL of tetramethylammonium hydroxide (25% w/v in methanol), followed by centrifugation and redissolution in 120 µl DMSO. M3-qdots in DMSO were then eluted through a G25 Sephadex column equilibrated with distilled water, before being dialyzed overnight against a 50 mM borate + 50 mM NaCl pH 7.3 buffer to remove excess peptides. Post-dialysis, M3-qdots were subject to an extra cleaning step on a G-50 spin column (Harvard Apparatus) equilibrated with 50 mM borate + 50 mM NaCl pH 7.3 buffer. M3-qdots at ~ 200 nM were kept at 4°C until further use.

***In vitro* complementation kinetics in solution and "on beads" complementation assays**. The complementation kinetics of biotin-M3 with GFP 1-10 in bacterial extract were studied for both non-limited amounts of GFP 1-10 (biotin-M3 at 180 pmoles and 18 pmoles) and for limited amount of GFP 1-10 (excess biotin-M3 at 18 nmoles). The assay was done in a 96-well microplate and in triplicate by mixing 18 nmoles, 180 pmoles or 18 pmoles of biotin-M3 with GFP 1-10 bacterial extract in TNG buffer. The final volume in each well was 57 µl. The microplate was incubated at 30°C and GFP fluorescence measurements were done every five minutes for the first hour, every ten minutes for the second hour and every twenty minutes in the last hour for a total length of 3 hours. Measurements were done on a Tristar LB 941 fluorescence reader (Berthold Technologies) with an excitation at 485 nm and an emission at 535 nm. Data points are reported as mean value of triplicates (± standard error) after background correction (GFP 1-10 in bacterial extract without biotin-M3). Over the 3 hours measurement there was less than 10 % loss in total GFP signal as determined with a control GFP solution.

In order to test the efficiency of *in vitro* complementation between GFP 1-10 and synthetic M3 peptides under restricted conformational freedom, biotin-M3 peptides were affixed to agarose beads via biotin/streptavidin interaction and further incubated with GFP 1-10 in bacterial extract. In brief, Alexa-647 labeled streptavidin was obtained by incubating 2.0 mg/ml of streptavidin (SAV, Sigma) in PBS pH 7.4 with a 6-fold molar excess of Alexa Fluor 647-NHS (Invitrogen) in DMSO, for 30 min at room temperature. The SAV-A647 conjugate was cleaned on two G-25 spin columns (Harvard Apparatus) equilibrated with PBS and then incubated for 20 min with biotinylated agarose beads (Thermo Scientific). The SAV-A647 modified beads were washed four times with PBS, before incubation for 15 min with biotin-M3 (4 mg/ml) or biotinylated FCC-M3 peptides (1 mg/ml) at 37°C. FCC-M3 peptides were biotinylated by incubation of 2 mM FCC-M3 with equimolar amount of maleimide-PEG$_{10KDa}$-biotin (Rapp polymer) for 30 min at room temperature in DMSO. The reaction was quenched for 120 min by addition of excess cysteine in PBS pH 7.4 and biotin-PEG$_{10KDa}$-FCC-M3 peptides were cleaned on two G-25 spin columns before incubation with SAV-A647 modified beads. SAV-A647 beads modified with both types of biotinylated M3 peptides were washed four times with PBS and incubated with 100 µl of GFP 1-10 in bacterial extract at 37°C for 45 min. After a series of six final washes in PBS, the beads were imaged on a Leica TCS SP2AOBS confocal microscope (Leica) equipped with a 100 x/1.4 NA oil immersion objective. GFP was excited at 488 nm and fluorescence was detected in an emission window at 495-535 nm. SAV-A647 was excited at 633 nm and fluorescence was detected in an emission window at 650-750 nm.

Native gel electrophoresis and gel shift assays. The analyses of split-GFP complementation by native gel electrophoresis were done using 1% agarose gels in a 40 mM Tris acetate, 1 mM EDTA, pH 8.3 buffer (TEA). For the gel of figure 1b, 130 µM of Cys-M3 peptides were incubated in TNG buffer (Lane 1) or with equimolar amount of GFP 1-10 ("Fold 'n' Glow" reagent, Lane 3) in a volume of 10 µl, at 37°C and for 150 min. Electrophoresis was done for 40 min at 170 V in TEA. For the gel shift assay of figure 1c, non-reactive, hydrolyzed Alexa Fluor 647 maleimide (Fig. S2, A647) at 2 µM was incubated with 135 µM of GFP 1-10 ("Fold 'n' Glow" reagent, Lane 1). M3-A647 conjugate at 1.5 µM was incubated in TNG buffer (Lane 2). M3-A647 conjugate at 1.5 µM was incubated with 135 µM of GFP 1-10 ("Fold 'n' Glow" reagent, Lane 3). In a binding competition assay, 235 µM of biotin-M3 (~150 fold excess) was mixed with 1.5 µM of M3-A647 conjugate and incubated with 135 µM of GFP 1-10 ("Fold 'n' Glow" reagent, Lane 4). All samples (10 µl volume) were incubated for 18 hours at 4°C and electrophoresis was done for 20 min at 170 V in TEA buffer. All gels were imaged on a FUJI FLA 3000 gel scanner (Fuji Film). GFP was detected using a laser excitation at 473 nm and detection through a 520 nm long pass filter. M3-A647 was detected with a laser excitation at 633 nm and detection through a 670 nm long pass filter. Förster resonance energy transfer (FRET) of GFP to M3-A647 was detected by laser excitation at 473 nm and detection through a 670 nm long pass filter.

In vitro **single molecule imaging of complemented GFP and i***n vitro* **imaging of split-GFP complementation.** Complemented GFP-biotin was obtained by incubation of 35 µM M3-biotin with 20 µl of GFP 1-10 in bacterial extract at 37°C for 30 min and purification by size exclusion HPLC (GFP-biotin peak at t=33.1 min, Fig. S1). The purified GFP-biotin was diluted in PBS buffer to single molecule concentrations and allowed to bind non-specifically on KOH treated glass coverslips before imaging in PBS buffer. Imaging was done by total internal reflection fluorescence (TIRF) microscopy with a inverted microscope equipped with an x100, 1.45NA objective (Olympus) and a QuantEM:512SC EMCCD camera (Photometrics). Single molecules of GFP were detected using a 488nm laser excitation (0.2 kW/cm^2), a 475DF40 excitation filter (Chroma Technology), a 495DRLP dichroic mirror (Omega Optical) and a 535DF40 emission filter (Chroma Technology). Multiple fields-of-view were imaged continuously for 25 s using an integration time of 60 ms per frame. The fluorescence intensity distribution of single GFPs was obtained from fluorescence time trace analysis of 152 individual molecules using a homemade software (AsteriX) (4) written in Labview (National Instruments). The distribution corresponds to the cumulative integrated fluorescence intensity within a 3x3 pixels region centered on each GFP spot for the whole length of acquisition, including periods with no GFP signal after photobleaching (background photons). For *in vitro* imaging of split-GFP complementation, KOH-treated glass coverslips were functionalized with biotin-M3 peptides. KOH treated glass coverslips (22 Ø mm) were first modified with 2.5 % of 3-aminopropyl triethoxy silane (Sigma) in methanol for 10 min. After multiple washes with distilled water, each coverslip was further incubated with 100 µl of 250 nM biotinylated anti-avidin antibody (Vector Laboratories) in PBS for 10 min. After multiple washes with PBS, the coverslips were incubated with 200 µl of 100 pM avidin (Sigma) for 5-10 min, washed with PBS and 200 µl of biotin-M3 peptides at 220 nM was applied for 10 min. After washes with PBS, the coverslips functionalized with biotin-M3 peptides were mounted on the TIRF microscope and 300 µl of GFP 1-10 in bacterial extract previously desalted against PBS on a PD MiniTrap G-25 column (GE Healthcare) was applied. Every 10 min, during the complementation reaction, 4-5 different fields-of-view were imaged continuously for 15s with a 488 nm excitation (0.6 kW/cm^2) and an integration time of 30 ms per frame. Optical filters and mirrors were as described above. All steps, including imaging were done at room temperature. Images from

representative fields-of-view at different incubation times are shown as maximum intensity projection of 15s videos. Fluorescence intensity time traces of complemented GFP-biotin were obtained by integrating the fluorescence intensity within a 4x4 pixels region centered on each GFP.

Construction and cloning of GFP 1-10 fusion proteins. For the expression of the transmembrane GFP 1-10 fusion protein, a pcDNA3 plasmid encoding the split-GFP 1-10 fragment N-terminally fused to a piece of the human CD4 glycoprotein was a kind gift of Alain Joliot. This fusion protein, described as CD4-2::spGFP1-10 in Feinberg et al. (5), was inserted into the mammalian pcDNA3 expression vector by HindIII and EcoRV ligation. This construct is made of an N-terminal PAT-3 beta-integrin secretion signal (6) followed by GFP 1-10 fused in frame to the truncated human CD4 with only two of the four immunoglobulin domain regions, the full transmembrane domain, and only the first seven amino acids of the cytoplasmic tail domain (GFP 1-10-CD4). This truncated CD4 comprises the palmitoylation domain (7) and the adjacent positive RHRRR amino acids sequence (8) necessary for its association with membrane raft microdomains at the plasma membrane. For the expression of the glycophosphatidylinositol anchored GFP 1-10 attached to the upper leaflet of the plasma membrane, we designed a "humanized" synthetic version of the GFP 1-10 cDNA and fused it to a piece of the human CD14 receptor that contains a C-terminal propeptide for GPI lipid anchor modification (4). This construct is made of an N-terminal archetypal eukaryotic secretion signal borrowed from chicken avidin (4) followed by the humanized GFP $1-10_{(h)}$ fused in-frame to the truncated human CD14 (GFP $1-10_{(h)}$-GPI). Humanized codon usage for GFP $1-10_{(h)}$ was similar to that employed by Zolotukhin et al. (9) and the 16 mutations necessary for split-GFP 1-10 OPT (10) were kept. To facilitate subcloning, we also included an upstream Hind III restriction site followed by an appropriate Kozak consensus sequence at the start codon as well as a series of restriction sites including XbaI downstream of the stop codon. The designed gene was synthesized (Genescript) and provided into a pUC57 bacterial expression plasmid. The full GFP $1-10_{(h)}$-GPI synthetic gene was extracted from pUC57 as a HindIII-XbaI fragment and sub-cloned into a pcDNA3 mammalian expression vector previously digested with HindIII-XbaI. For the expression of the caveolin-1-GFP 1-$10_{(h)}$ fusion protein (cav1-GFP $1-10_{(h)}$), we replaced EGFP from a pCav1-EGFP-N1 plasmid encoding the canine caveolin-1 fused to EGFP (4), by GFP $1-10_{(h)}$. The GFP $1-10_{(h)}$ fragment from GFP $1-10_{(h)}$-GPI in pCDNA3 was PCR amplified with the following forward primer to add a 5'-AgeI restriction site: sense, 5'atccaccggtcgccaccatgtccaaaggagaagaactg3', and the following reverse primer to add a 3' stop codon and a XbaI restriction site: antisense, 5'cgagcctctagattatgttcctttttcatttggatc3'. The pCav1-EGFP-N1 plasmid, which contains the caveolin-1 coding sequence inserted by EcoRI-SacII ligation into a pEGFP-N1 (Clontech Laboratories), was amplified in a Bam⁻ bacterial strain to avoid methylation of the XbaI restriction site downstream of EGFP. The EGFP coding sequence was then removed by digestion of with Age1-Xba1. The PCR-amplified GFP $1-10_{(h)}$ fragment was similarly digested by Age1-Xba1, gel-purified and ligated to the open pCav1-…-N1 plasmid to obtain a pCav1-GFP $1-10_{(h)}$-N1 mammalian expression plasmid, encoding caveolin-1 fused in-frame to GFP $1-10_{(h)}$. All gene constructs were verified by DNA sequencing.

Immunolabeling of caveolin-1-GFP $1-10_{(h)}$. Primary rabbit anti-caveolin-1 antibodies were obtained from BD Bioscience (#610060) and primary mouse anti-GFP antibodies were obtained from Clontech (#632375). Secondary polyclonal goat anti-rabbit Alexa 488 conjugated antibodies (#A11008) and secondary polyclonal donkey anti-mouse Alexa 647 conjugated antibodies (#A31571) were obtained from Invitrogen. U20S cells were grown on fibronectin-coated coverslip to 60-70% confluency and

transiently transfected with pCav1-GFP 1-10$_{(h)}$-N1, 48 hours before fixation. Cells were washed with PBS at 37°C, and fixed on ice for 10 min with -20°C cold methanol:acetone 1:1 (v/v). Cells were rehydrated by multiple washed with PBS at room temperature and further blocked for 30 min in PBS + 10% FCS. Both primary antibodies were then simultaneously incubated on cells in PBS + 10% FCS for 40 min and at room temperature. Cells were then extensively washed in PBS + 10% FCS before incubation with both secondary antibodies simultaneously. Specificity of labeling and absence of antibody cross-reactivity was verified by control experiments omitting either the primary or the secondary antibodies. Cells were imaged on a spinning disc confocal microscope at the ventral plasma membrane and at different focal plans for 3D reconstructions (video S4).

Cell transfection, staining and imaging. All cell lines (U20S, HEK and COS-7) were cultured in DMEM + 10% FCS at 37°C in a humidified atmosphere containing 5 % CO$_2$. Transient transfections were performed with lipofectamine (Invitrogen) or fugene (Roche Biosciences) reagents. Two stable multiclonal U20S cell lines constitutively expressing GFP 1-10-CD4 and GFP 1-10$_{(h)}$-GPI respectively were obtained by linearization of the corresponding pcDNA3 plasmids by PciI and BglIII digestion respectively, fugene transfection and selection with G418. To visualize cells expressing cav1-GFP 1-10$_{(h)}$ prior to microinjection or Pep1 translocation of the complementary M3 peptides, the pCav1-GFP 1-10$_{(h)}$-N1 plasmid was transiently co-transfected with either a plasmid encoding the nuclear CFP-LacI-NLS or a plasmid encoding the actin-binding peptide mCherry-LifeAct (ABP-mCherry). No co-transfection was performed for immunolabeling of cav1-GFP 1-10$_{(h)}$.

For ensemble extracellular cell staining with biotin-M3, Cys-M3 or FCC-M3 peptides, synthetic M3 peptides were dissolved in DMSO to about 14.0 mM and the solution was further diluted to 3.5 mM in TN buffer pH 7.2. Residual DMSO was eliminated by elution of the peptide solution on G-10 spin columns (Harvard Apparatus) equilibrated with TN buffer pH 7.2. The peptide solution was conserved at 4°C. Cells grown on fibronectin-coated glass coverslips to 70-80% confluency were briefly washed with Tyrode's buffer (136 mM NaCl, 10 mM KCl, 0.4 mM MgCl$_2$, 1.0 mM CaCl$_2$, 5.6 mM Glucose, 10.0 mM Hepes, pH 7.8) at 37°C, and incubated with M3 peptides diluted to 50 µM in Tyrode's buffer + 5-10% FCS at 37°C for 45-60 minutes. In some experiments, Trolox (Sigma) at 2 mM was added to the M3 peptide/Tyrode's buffer/FCS solution. After a brief wash with Tyrode's buffer, wide field or confocal fluorescence imaging of live cells was performed in HEPES buffered HBSS (145 mM NaCl, 5 mM KCl, 1.2 mM MgSO$_4$, 2.0 mM CaCl$_2$, 1.2 mM NaH$_2$PO$_4$, 10 mM Glucose, 20.0 mM Hepes, pH 7.6) or Tyrode's buffer at 37°C, using a thermostated cell imaging chamber (20/20 Technology). For double staining of living cells with anti-GFP antibodies, Alexa-647 labeled anti-GFP rabbit IgG (Invitrogen) was added at 2 µg/ml for 20-30 min before the end of the incubation period with M3 peptides. For double staining of living cells with the SAV-A647 conjugate, cells were washed with Tyrode's buffer at 37°C to remove the FCS after 60 min incubation with M3 peptides, and further incubated at 37°C in 1 ml HBSS + 1% BSA containing 35 nM of SAV-A647 for 20 min. After washes, cells were imaged at 37°C as above. For ensemble extracellular cell staining with fluorescent the M3-A647 peptide conjugate, cells were treated as above, M3 peptides were replaced by 1.5 µM of M3-A647, and anti-GFP staining was omitted. For cell staining with M3-qdots, cells were treated as above, M3 peptides were replaced by 30 nM of M3-qdots, and anti-GFP staining with Alexa-647 labeled anti-GFP rabbit IgG was performed for only 5 min. Diffusing qdots were imaged by wide-field fluorescence microscopy with a 100 ms/frame integration time.

For ensemble intracellular staining with biotin-M3 peptides, U2OS cells grown at 70-80% confluency on fibronectin-coated coverslip and transiently transfected with pCav1-GFP 1-10$_{(h)}$-N1 and

ABP-mCherry plasmids for 48 hours, were briefly washed in HBSS buffer or DMEM without phenol red, and mounted in a cell-imaging chamber on a fluorescence microscope equipped with a microinjector (Femtojet, Eppendorf) and FemtotipII microinjection capillaries. Cells were injected for 1.5 s with a few hundreds of femtoliters of a 700 µM biotin-M3 solution in PBS (~25 µM final intracellular concentration) + 0.01% BSA and imaged by wide-field or TIRF microscopy at 37°C, 45 min after microinjection.

For extracellular single molecule imaging of split-GFP fusion proteins, U2OS cells stably expressing GFP 1-10-CD4 or GFP 1-10$_{(h)}$-GPI were grown on fibronectin-coated glass coverslips to 70-80% confluency, briefly washed with Tyrode's buffer, and mounted in a cell-imaging chamber at 37°C in Tyrode's buffer on a TIRF microscope. Biotin-M3 peptides were added once, at 1.8 µM on cells during TIRF imaging at the beginning of the experiment. Cells were then continuously imaged for 1 minute with constant laser excitation and a 60 ms/frame integration time, every 5 minutes. During periods where no data was acquired (4 minutes) the excitation laser was switched off. After 45 minutes of imaging an additional 18 µM of biotin-M3 peptides was added again on cells and imaging was performed every 5 minutes as before.

For intracellular single molecule imaging of cav1-GFP 1-10$_{(h)}$, U2OS cells grown at 70-80% confluency on fibronectin-coated coverslip and transiently transfected with pCav1-GFP 1-10$_{(h)}$-N1 and the CFP-LacI-NLS plasmid for 48 hours were briefly washed in HBSS buffer and mounted in a cell-imaging chamber in HBSS buffer on a TIRF microscope equipped with a microinjector (Femtojet, Eppendorf) and FemtotipII microinjection capillaries. Cells were microinjected at room temperature for 0.3 s with a few tens of femtoliters of a filter sterilized 1.8 mM biotin-M3 solution in PBS (~5 µM final intracellular concentration) containing 5 µM of biotin-Alexa 647 conjugate used as an microinjection marker and immediately imaged. Biotin-Alexa 647 was synthesized and purified as previously reported (11). Cells were continuously imaged for 30 seconds with continuous 488 nm laser excitation and a 100 ms/frame integration time, at 3, 5 and 10 minutes after microinjection. During periods where no data was acquired the excitation laser was switched off.

For coincidence single molecule imaging between GFP and the bound M3-A647 peptide in complemented A647-GFP-CD4, cells were stained as for extracellular ensemble cell staining with the M3-A647 conjugate but only cells with low GFP 1-10-CD4 expression levels were imaged. For these cells, single diffusing A647-GFP-CD4 complexes could easily be observed within 2-3 frames of imaging after which some of the molecules had bleached. Imaging was done by TIRF, with simultaneous dual-excitation at 488 nm and 638 nm, dual-color detection and a 60 ms/frame integration time.

For FRET imaging of A647-GFP-CD4 complexes, U2OS cells stably expressing GFP 1-10-CD4 were incubated with 2.5 µM M3-A647 peptide conjugate for 40 minutes at 37°C, washed with Tyrode's buffer and imaged at 37°C with a 60 ms/frame integration time on the TIRF microscope and using a single excitation at 488 nm and dual-color detection. Dual-color single molecule tracking by single pair FRET was done on cells having low GFP 1-10-CD4 expression.

For FRET imaging at high concentrations of M3-A647 conjugate, U2OS cells stably expressing GFP 1-10-CD4 were mounted in a cell-imaging chamber on the TIRF microscope in Tyrodes's buffer and at 37°C. 700 nM of M3-A647 peptide conjugate was added directly in the imaging buffer and imaging was started after 20 minutes incubation without washes. TIRF imaging was done with an integration time of 60 ms/frame, using a single excitation at 488 nm and dual-color detection to observe FRET. A single TIRF excitation at 638 nm and dual-color detection was also used to image the excess of M3-A647 conjugate in the cell media.

Optical set ups. Wide-field epifluorescence imaging was performed on an IX70 Olympus inverted microscope equipped with a x100, 1.45 NA objective, a UV lamp at the back entry port (Rapp Optoelectronic) and appropriate optical filters for imaging CFP (exc: 440AF10, dichroic: 455DRLP and em: 480AF20), GFP (exc: 475AF40, dichroic: 515DRLP and em: 535AF45), mCherry (exc: 580DF30, dichroic:600DRLP and em: 620DF30) or Alexa Fluor 647 (exc: 3RD/570-645, dichroic: 650DRLP and em: 690DF40). Fluorescence was detected on the right-side exit port of the microscope with a QuantEM:512SC EMCCD camera (Photometrics).

TIRF imaging was performed on the same inverted IX70 Olympus microscope equipped with a x100, 1.45 NA objective and using a custom-built optical set up to bring laser lines to the left-side port entry of the microscope. In brief, the 488 nm and 638 nm laser lines of a solid state laser (Melles Griot) and a diode laser (Microlasers Systems) respectively were coupled into an acousto-optical tunable filter (AA Opto Electronic), circularly polarized with a λ/4 wave plate, collimated, expanded and refocused at the back focal plane of the objective lens. Total internal reflection was obtained using a set of two mirrors (one mounted on a micrometer stage) to move the beam away from the optical axis and reach the critical angle. For simultaneous excitation, laser lines were sent through a multi-bandpass FF01-390-482-563-640 excitation filter (Semrock) and reflected on a dual-band FF500/646-Di01 dichroic mirror (Semrock). Fluorescence emitted from the samples was collected by the same objective lens and redirected to the EMCCD. For simultaneous dual-color detection, the fluorescence light path was divided into a green and red path using a DV2 Dual-view system (Photometrics), equipped with a green D535/40M emission filter, a 565 dichroic mirror and a red 695DF55 emission filter. Green and red images were adjusted to cover equal areas on each side of the EMCCD. The size of pixels in images was determined by imaging a micrometer reticle. 40 nm diameter TransFluoSphere beads (488/685 nm, Invitrogen) were also imaged to align green and red images and correct for chromatic aberrations before image overlay. Errors in image alignment depended on the exact location in the field of view and were approximately of 1 pixel (~100 nm) in the worst case.

Confocal imaging was performed on a confocal Leica TCS SP2AOBS microscope as described above, or on a Leica DM5000B microscope equipped with a x100, 1.4 NA objective, a CSU10 spinning disc confocal scanner system (Yokogawa), 491 nm (Cobolt) and 635 nm (Coherent) lasers, and a CoolSnap HQ CCD camera (Photometrics).

Tracking and diffusion analysis of single split-GFPs, single fluorophores and single qdots tracking in living cells. All single molecule tracking and subsequent analyses were done using a previously described series of homemade software called AsteriX and written in Labview (4). In brief, the center of individual point-spread-functions (PSF) corresponding to single complemented split-GFPs, single fluorophores or single qdots were fitted with a 2-dimensional Gaussian profile. A semi-automatic fitting mode repeats this process frame after frame. A single trajectory is represented by the fitted positions, connected by a straight line. The mean trajectory lengths are reported in second ± standard deviation of the mean (Supplementary table). The localization uncertainty σ for a single molecule was estimated as previously reported (12, 13), with:

$$\sigma_0{}^2 = \frac{S_0{}^2 + a^2/12}{N} + \frac{8\pi S_0{}^4 b^2}{a^2 N^2} \quad (1)$$

where N is the number of photons recorded in the fitted PSF, a is the pixel size, b is the background noise standard deviation and S_0 is the standard deviation of the PSF evaluated with:

$$S_0 = 0.21 \frac{\lambda}{NA} \quad (2)$$

where λ is the emission wavelength and *NA is* the numerical aperture of the objective lens. As previously described (14), σ_0 was further corrected by (i) an excess factor noise of 1.4 to account for the electron multiplication process of the EMCDD and by (ii) an uncertainty factor due to diffusion such that:

$$\sigma = 1.4 \, \sigma_0 \sqrt{1 + \frac{Dt_E}{S_0^2}} \quad (3)$$

where D is the diffusion coefficient and t_E is the camera exposure time. To obtain a representative value of the localization uncertainty for different molecules, a mean localization uncertainty σ_m was evaluated for 100 single molecules in different video frames and at different positions in the plasma membrane of 4 or 5 cells. The mean localization uncertainty σ_m is reported in nanometer ± standard deviation of the mean (Supplementary table).

As mentioned previously intensity time traces for immobilized single molecules where obtained by integrating the fluorescence intensity within a selectable number of pixels (usually 3x3 or 4x4 pixels) around the PSF center. Fluorescence intensity distribution histograms correspond to the cumulative integrated intensity of multiple intensity time traces. For diffusing molecules, intensity time traces were obtained by integrating the fluorescence intensity within a selectable number of pixels around the PSF center, along the diffusion trajectory.

The AsteriX software also allows exporting a diffusion trajectory tracked in one channel (e.g. GFP channel) to a second channel acquired simultaneously (e.g. Alexa 647 channel). Thus, after image correction and alignment, it is possible to obtain M3-A647 intensity time traces along the diffusion path of a complemented GFP 1-10 fusion protein. Using this approach, single pair FRET signals from diffusing A647-GFP-CD4 proteins were obtained by correlating fluorescence intensity time traces from both Alexa 647 and GFP channels along the diffusion trajectory of single proteins.

Diffusion analyses were performed as previously described (4) on ensemble mean square displacement curves (MSD, Fig. S6) and on ensemble histograms of probability distribution of the square displacements (15) (P_r^2). Diffusion coefficients were obtained by fitting the MSD and P_r^2 curves on the first four non-zero points of the curves (D_1-D_4), using a simple Brownian diffusion model with measurement error: $4\sigma^2 + 4Dt$. Diffusion coefficients are reported in $\mu m^2/s$ ± standard deviation of the fit. Analyses by P_r^2 also provide an additional set of parameters (α_i) which indicates the fraction of each subpopulation detected. These fractions are reported in percentage (Supplementary table). Note that we used Occam's razor principle when looking for subpopulations in P_r^2 histograms, keeping the lowest number of subpopulations that would properly describe the histograms.

Supplementary video captions

Video S1: Single molecule imaging of complemented split-GFP *in vitro*. GFP 1-10 are complemented *in vitro* with synthetic biotin-M3 peptides and deposited on a clean glass coverslip. Upon single step photobleaching the GFPs sequentially disappear from the imaging field. Imaging is performed by TIRF with a 60 ms/frame integration. Video playback: 30 frames/second.

Video S2: TIRF imaging of complemented GFP 1-10-CD4 proteins in the plasma membrane of U20S cells. Cells are incubated with 1.8 μM of biotin-M3 for 45 min at 37°C. The complementation is highly specific of the GFP 1-10-CD4 expressing cell and individual GFP-CD4 proteins diffuse in the plasma membrane. Acquisition: 60 ms/frame. Video playback: 30 frames/second.

Video S3: Wide-field fluorescence imaging of GFP 1-10$_{(h)}$-GPI proteins for long complementation times. GFP is imaged for a COS-7 cell expressing GFP 1-10$_{(h)}$-GPI and incubated at 37°C for 48 hours with 25 μM of biotin-M3 complementary peptides in HBSS buffer + 20% FCS. Imaging frame rate: 60 ms/frame. Video playback: 30 frames/second.

Video S4: Immunostaining of endogenous caveolin-1 and caveolin-1-GFP 1-10 fusion proteins in U2OS cells. 3-D projections of confocal sections for U2OS cells immunostained for endogenous caveolin-1 (anti-cav1, left) or for GFP 1-10 after expression of cav1-GFP 1-10 (anti-GFP, right). In both cases, a typical punctuated pattern corresponding to caveolae-associated caveolin-1 is observed at the cell plasma membrane.

Video S5: TIRF imaging of complemented intracellular caveolin-1-GFP 1-10 fusion proteins in living cells. Simultaneous dual-color TIRF imaging of U2OS cells co-expressing cav1-GFP1-10$_{(h)}$ and ABP-mCherry, after complementation by microinjection of synthetic M3 peptides (top) or no microinjection (bottom). The punctuated pattern of caveolae-associated and complemented cav1-GFP is visible at the ventral plasma membrane of the injected cell (zoom). Imaging is performed with a 100 ms/frame integration. Video playback: 30 frames/second. Note: The slight fluctuations at the beginning are due to a realignment of the TIRF excitation field.

Video S6: CALM imaging of individual transmembrane GFP 1-10-CD4 in U2OS cells. The ventral plasma membrane of an expressing cell (top) and a non-expressing cell (bottom) are repeatedly imaged every 5 minutes for about 1 minute, before, during and after addition of complementary M3 peptides at 1.8 μM the imaging buffer. After 45 min imaging, the same expressing cell (top) is imaged in the same manner following the addition of 18 μM complementary M3 peptides. The timing is provided in minute:second format and hour:minute:second format after 60 minutes. Imaging is performed with a 60 ms/frame integration. Video playback: 30 frames/second.

Video S7: CALM imaging of individual lipid-anchored GFP 1-10$_{(h)}$-GPI proteins in U2OS cells. The ventral plasma membranes of an expressing cell (+) and a non-expressing cell (-) are imaged after 25 min incubation with 5 μM of M3 complementary peptides at 37°C. Notice the very high specificity of labeling for the expressing cell only. Imaging is performed with a 60 ms/frame integration. Video playback: 30 frames/second.

Video S8: CALM imaging of individual intracellular cav-1-GFP$_{(h)}$ proteins in U2OS cells. The ventral plasma membranes of an expressing and microinjected cell (+ and *) and that of an expressing but not microinjected cell (+) are imaged at regular intervals (3, 5 and 10 min) for 30 seconds under continuous 488 nm laser excitation and following microinjection of M3 peptides. Notice the increasing amount of single cav1-GFP$_{(h)}$ lighting up at the membrane of the microinjected cell with increasing incubation times. Imaging is performed with a 100 ms/frame integration. Video playback: 30 frames/second.

Video S9: Simultaneous dual-color TIRF imaging of diffusing complemented A647-GFP-CD4 proteins in the plasma membrane of a U2OS cell. Imaging is performed by dual-color laser excitation at 488 and 638 nm and dual-color detection of A647-GFP-CD4 in separate GFP-CD4 and M3-A647 channels. Images from both channels have been overlaid after correction for alignment and chromatic aberrations (see Methods). Imaging is performed with a 100 ms/frame integration. Video playback: 10 frames/second.

Video S10: Co-incident single molecule detection of complemented A647-GFP-CD4 proteins by dual-color TIRF imaging in U2OS cells. A region of interest from supplementary video S9 showing two diffusing A647-GFP-CD4 transmembrane proteins is selected. For both proteins, GFP photobleaches in a single step before the Alexa 647 fluorophore. The point spread functions of GFP-CD4 and M3-A647 have been intentionally expanded to facilitate visualization. Imaging is performed with a 100 ms/frame integration. Video playback: 10 frames/second.

Video S11: Wide-field fluorescence imaging of M3-qdots targeted by CALM to GFP 1-10-CD4 proteins in U2OS cells. M3-qdots emitting at 545 nm specifically bind to the expressing cell (top right). The lateral membrane diffusion of single qdot-GFP-CD4 complexes at the cell surface and along filopodias is visible. Imaging is performed with a 100 ms/frame integration. Video playback: 30 frames/second.

Video S12: Cell imaging by complementation-induced intramolecular single pair Förster resonance energy transfer (spFRET). U2OS cells stably expressing the transmembrane GFP 1-10-CD4 fusion proteins are complemented with fluorescent M3-A647 (left) or non-fluorescent M3-biotin (right) peptides and imaged by dual-color TIRF microscopy using only a 488 nm laser excitation. spFRET from A647-GFP-CD4 proteins leads to fluorescence emission in the Alexa channel (left), but is absent from biotin-GFP-CD4 proteins (right). Single A647-GFP-CD4 complexes can be seen diffusing in the membrane in both channels (left), with non-photobleached complexes entering the TIRF field from the cell edge. Imaging is performed with a 60 ms/frame integration. Video playback: 30 frames/second.

Video S13: Tracking individual proteins in living cells by intramolecular single pair Förster resonance energy transfer (spFRET). Two regions of interest showing individual complemented A647-GFP-CD4 proteins diffusing in the plasma membrane under continuous 488 nm laser excitation. The GFP and Alexa 647 channels have been overlaid to show that spFRET from single A647-GFP-CD4 proteins leads to fluorescence emission in both channels. In the left video, a diffusing A647-GFP-CD4 protein undergoes spFRET (yellow arrow) until GFP photobleaches in a single step, leading to disappearance of the protein. In the right video, another diffusing A647-GFP-CD4 protein undergoes spFRET (yellow arrow), until M3-A647 photobleaches in a single step. This leads to an arrest of spFRET and

an increase in GFP fluorescence (green arrow) before the protein fully disappears upon GFP single step photobleaching. Imaging is performed with a 60 ms/frame integration. Video playback: 30 frames/second. Note: the left video is repeated three times.

Video S14: Live cell tracking of individual proteins at very high probe concentrations. A U2OS cell is incubated with 0.7 μM M3-A647 without washing and imaged by TIRF with a single laser excitation at 488 nm. Complemented A647-GFP-CD4 proteins are specifically excited at 488 nm and undergo spFRET, as detected by the presence of diffusing and diffraction-limited fluorescence spots in the Alexa 647 channel. The lack of interference from the non-bound and large excess of M3-A647 peptides which are not excited at 488 nm, together with the good spatial and temporal separation between complemented single A647-GFP-CD4, facilitate tracking in the Alexa 647 channel by 2D-Gaussian fitting despite the presence of ~1 μM fluorophore in the imaging media. Imaging is performed with a 60 ms/frame integration. Video playback: 10 frames/second.
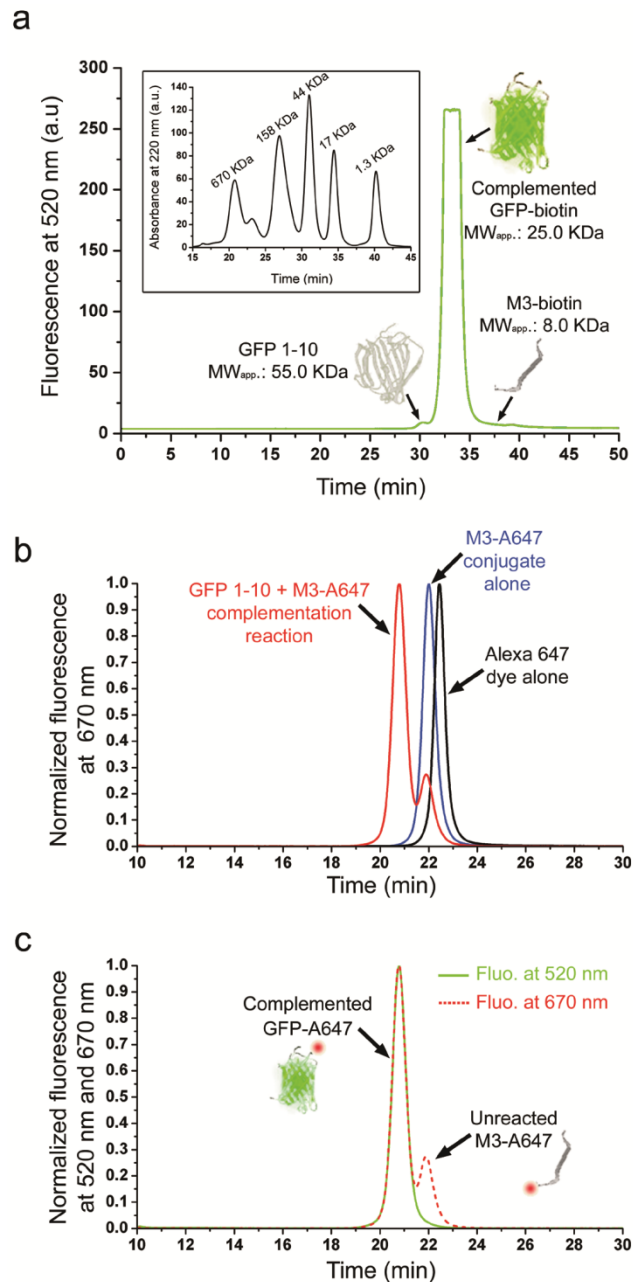
Fig. S1

Fig. S1: Size exclusion HPLC analysis of GFP 1-10 complemented *in vitro* with M3-biotin and M3-A647 peptides. (a) M3-biotin at 35 µM is incubated with 20 µl of GFP 1-10 in bacterial extract at 37°C for 30 min, the whole reaction is loaded on a Superdex^{TM} 200 HPLC column and the complemented GFP-biotin is detected by fluorescence at 520 nm as a single peak eluting at t=33.1 min (saturated green peak). In a different experiment GFP 1-10 from the bacterial extract and M3-biotin were detected by absorbance measurements at 220 nm and eluted at t=30.2 min and t=37.3 min respectively. The calibration of the column with a set of globular protein standards with known molecular weight (inset), indicates that the complemented GFP-biotin is a monomer with an apparent

molecular weight (MW$_{app.}$) of ~25.0 KDa, in agreement with that expected for monomeric GFP (~27 KDa) (16). GFP 1-10 elutes before the complemented GFP-biotin with a MW$_{app.}$ of 55.0 KDa as previously reported (10, 17). This probably reflects a dimerization of GFP 1-10 at high protein concentrations (16) or a non-globular form of GFP 1-10 with a possibly larger hydrodynamic radius than that of the complemented GFP-biotin. M3-biotin elutes after the complemented GFP-biotin, with a MW$_{app.}$ of 8.0 KDa, a value larger than the expected MW of 2.7 KDa because the Superdex^{TM} 200 column loses resolution for proteins and peptides below 10.0 KDa. **(b)** Fluorescence elution profile at 650 nm on a TSK-GEL G4000SW size exclusion HPLC column for unreacted Alexa Fluor 647 (black), purified M3-A647 peptide conjugate (blue) and for a complementation reaction made of 1.4 µM M3-A647 incubated with 135 µM of GFP 1-10 ("Fold 'n' Glow" reagent) at 4°C for 18 hours (red). As expected, the M3-A647 conjugate elutes before the free dye peak. For the complementation reaction, an early elution peak is observed together with a residual unreacted M3-A647 peak, indicating effective binding of M3-A647 to GFP 1-10. As confirmed in (c), this early peak corresponds to stable 1:1 GFP-A647 complexes. **(c)** The elution profile of the complementation reaction in (b) is further studied for GFP fluorescence (excitation at 488 nm and detection at 520 nm, green) and for M3-A647 fluorescence (excitation at 640 nm and detection at 670 nm, red dash). The early elution peak at 20.8 min (MW$_{app.}$ of 25.0 KDa) emits fluorescence in both the GFP and the M3-A647 channel, indicating that M3-A647 binds and effectively complements GFP 1-10 into a bright and stable 1:1 GFP-A647 complex emitting both GFP and far-red fluorescence. The presence of a residual unreacted M3-A647 elution peak despite the lengthy incubation and the large excess of GFP 1-10 indicates that only 1-2% of split GFP 1-10 in the "Fold 'n' Glow" reagent are reactive to complementation with M3-A647 (see also supplementary Fig. 10).
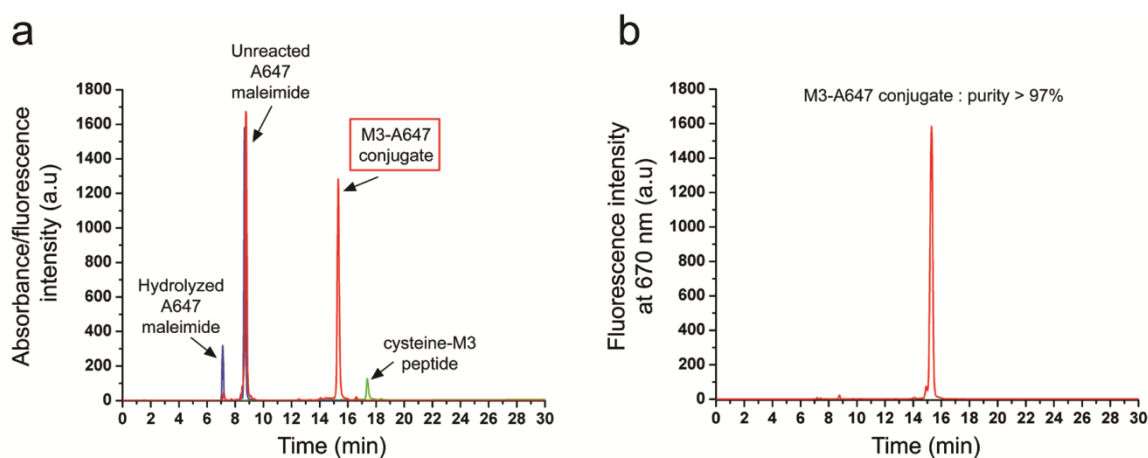
Fig. S2: Conjugation of Alexa Fluor 647 C_2-maleimide to cysteine-M3 peptide and HPLC purification. **(a)** Reverse phase HPLC elution profiles of free Alexa Fluor 647 maleimide (blue, fluorescence detection at 670 nm), free cystein-M3 peptides (green, absorbance detection at 280 nm) and unpurified conjugation reaction of Alexa Fluor 647 C_2-maleimide to cysteine-M3 peptides (red, fluorescence detection at 670 nm). The polar Alexa-647 fluorophore elutes early, in two peaks at ~17% and ~18.7% of the acetonitrile gradient (7 min and 8.7 min respectively), while the more hydrophobic cystein-M3 peptides elute later at ~27.5% of the gradient (17.5 min). Two main peaks are observed for the conjugation reaction: an unreacted Alexa Fluor 647 maleimide peak and the M3-A647 conjugate peak eluting at ~18.7% and ~25.5% of the gradient respectively (8.7 and 15.5 min respectively). The good separation between the M3-A647 conjugate and other reactants facilitates purification. **(b)** Purified M3-A647 peptide conjugate. The conjugate purity is better than 97% with no traces of free cystein-M3 peptides.
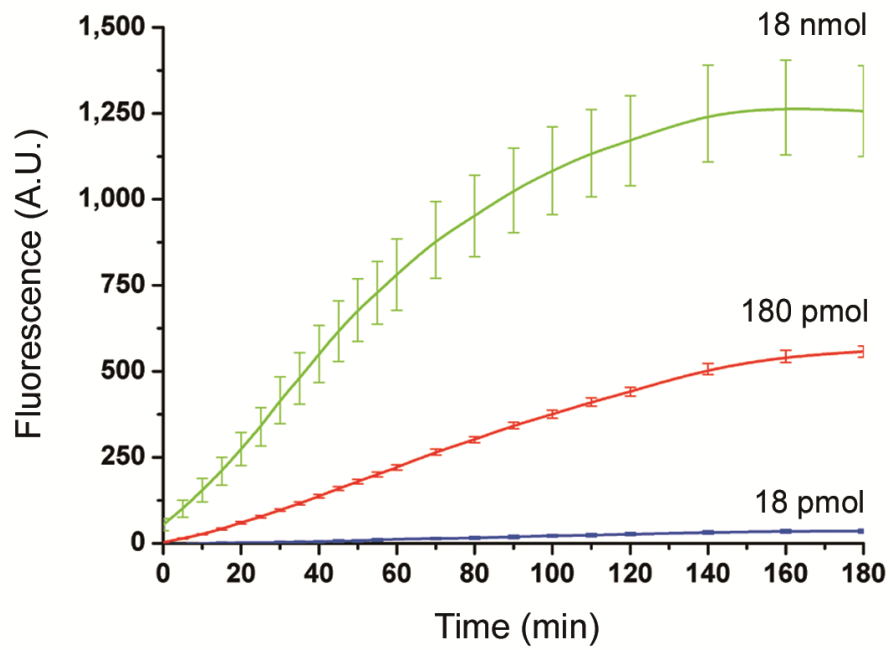
Fig. S3

Fig. S3: Split-GFP complementation kinetics in solution. Split-GFP complementation kinetics at saturating (18 nmol) and non-saturating (180 pmol and 18 pmol) amounts of biotin-M3 peptides in GFP 1-10 bacterial cytoplasmic extracts.

Fig. S4
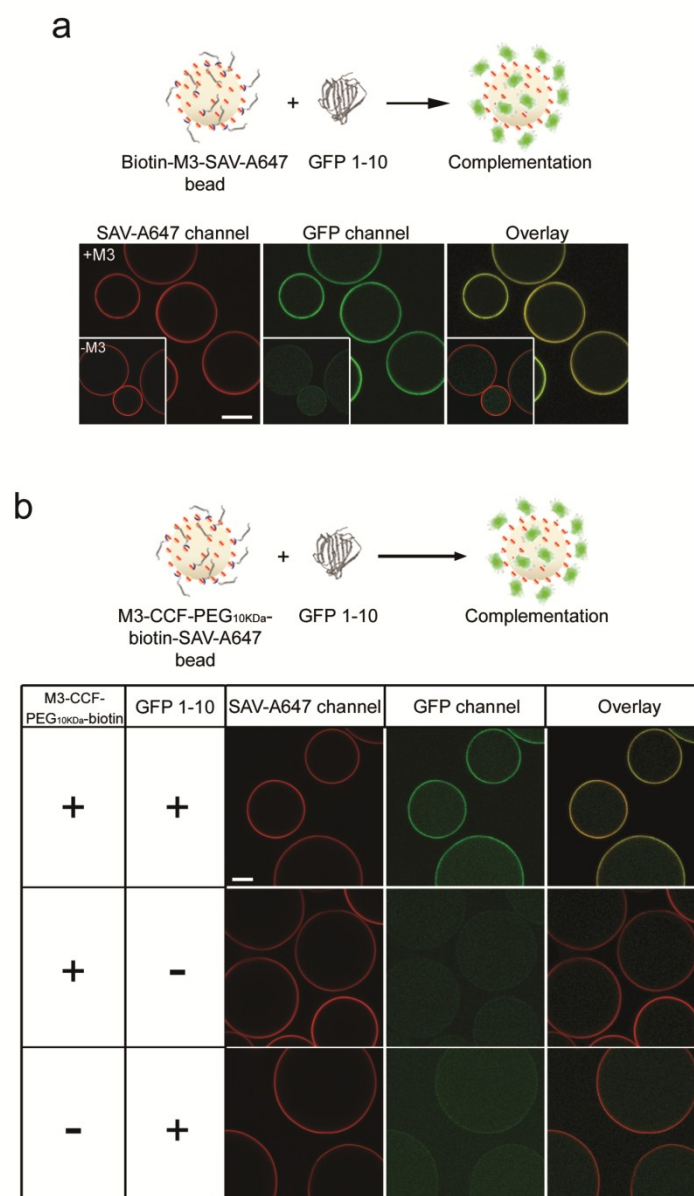
Fig. S4: "On beads" complementation of split-GFP with biotinylated M3 peptides. (a) Complementation of split-GFP with biotin-M3 peptides affixed to Alexa-647-streptavidin (SAV-A647) coated agarose beads. Incubation with GFP 1-10 induces GFP fluorescence at the beads' surface but no GFP is observed in the absence of biotin-M3 (inset). Scale bar: 25 μm. (b) Complementation of split-GFP with biotinylated FCC-M3 peptides. Incubation of GFP 1-10 with agarose beads modified with SAV-A647 and reacted with biotinylated FCC-M3 peptides induces the complementation of the split-GFP fragments and the appearance of GFP fluorescence at the beads' surface. In the absence of GFP 1-10 or biotinylated FCC-M3 peptides, no complementation is observed. Scale bar: 20 μm.
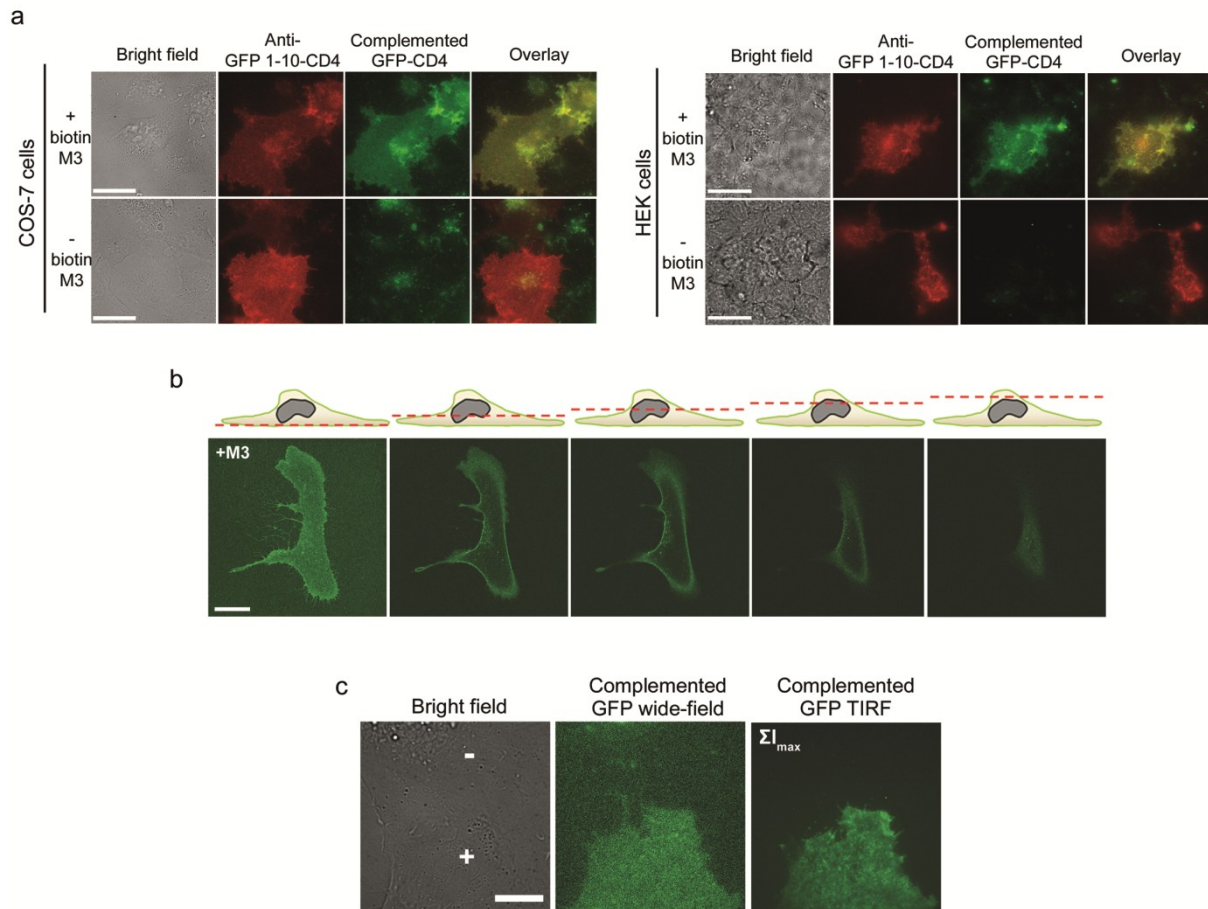
Fig. S5

Fig. S5: Plasma membrane complementation of GFP 1-10-CD4 proteins with synthetic M3 peptides. (a) Live COS-7 and HEK cells expressing GFP 1-10-CD4 are identified using a fluorescently labeled anti-GFP 1-10 antibody. Addition of M3 peptides (+ biotin-M3) induces the specific appearance of GFP to expressing cells only, as verified by the colocalizing anti-GFP and GFP signals (overlay). No GFP fluorescence is observed for expressing cells in the absence of complementing peptides (- biotin-M3). All scale bars: 20 μm. (b) Confocal fluorescence microscopy z-sectioning of a U20S cell expressing GFP 1-10-CD4 proteins and complemented with biotin-M3 peptide. GFP fluorescence is visible at the plasma membrane for different confocal optical sections through the cell (schematic, red dash-line). Scale bar: 25 μm. (c) Total internal reflection fluorescence (TIRF) imaging of M3 peptide complemented GFP 1-10-CD4 proteins in the plasma membrane of U2OS cells. The complementation is highly specific of the expressing cell (+), and no GFP signal is detected by wide-field fluorescence or TIRF imaging for the non-expressing cell (-). The TIRF image is a pixel-based maximum intensity projection image (ΣI_{max}) for all frames of a video available in supplementary video S2. Scale bar: 10 μm.
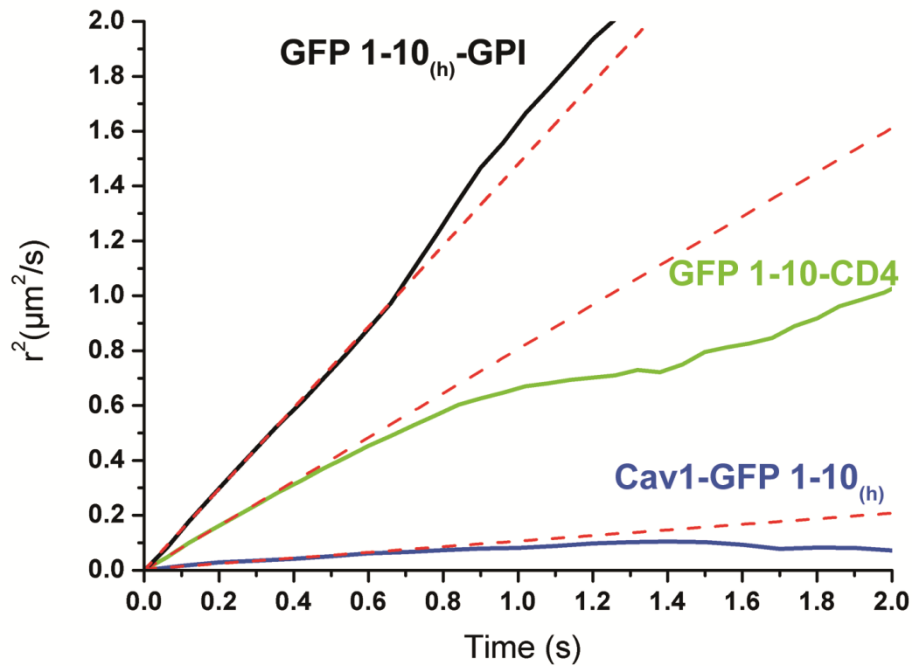
Fig S6: Analysis of the diffusion constants for complemented split-GFP fusion proteins from ensemble mean square displacements (MSD). MSD curves for GFP 1-10$_{(h)}$-GPI (black), GFP 1-10-CD4 (green) and cav1-GFP 1-10$_{(h)}$ (blue), are fitted to the first four non-zero points of the MSD curve (D1-D4, red dash-lines). The fitting formula is that of the free diffusion model with measurement error ($4\sigma^2+4Dt$, see Methods). Apparent ensemble diffusion constants for complemented GFP 1-10$_{(h)}$-GPI, GFP 1-10-CD4 and cav1-GFP 1-10$_{(h)}$ are 0.37 ± 0.02 μm^2/s, 0.21 ± 0.03 μm^2/s and 0.02 ± 0.003 μm^2/s respectively (see supplementary table).

Fig. S7
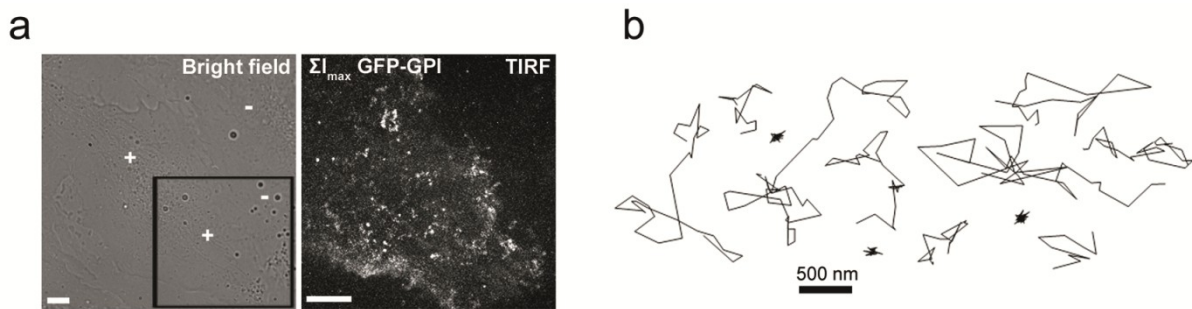
Fig. S7: TIRF imaging and single molecule tracking of complemented GFP 1-10$_{(h)}$-GPI proteins in the plasma membrane of U2OS cells. (a) An expressing cell (+) and a non-expressing (-) cell are imaged by TIRF after 25 min incubation with 5 µM of complementary M3 peptides at 37°C. The TIRF image is a pixel-based maximum intensity projection (ΣI_{max}) image for all frames of a video corresponding to the black square region of interest in the bright field image. This video is available in supplementary video S7. Scale bars: 5 µm. (b) Representative trajectories from single complemented GFP$_{(h)}$-GPI diffusing in the ventral plasma membrane of U2OS cells during CALM imaging.

Fig. S8
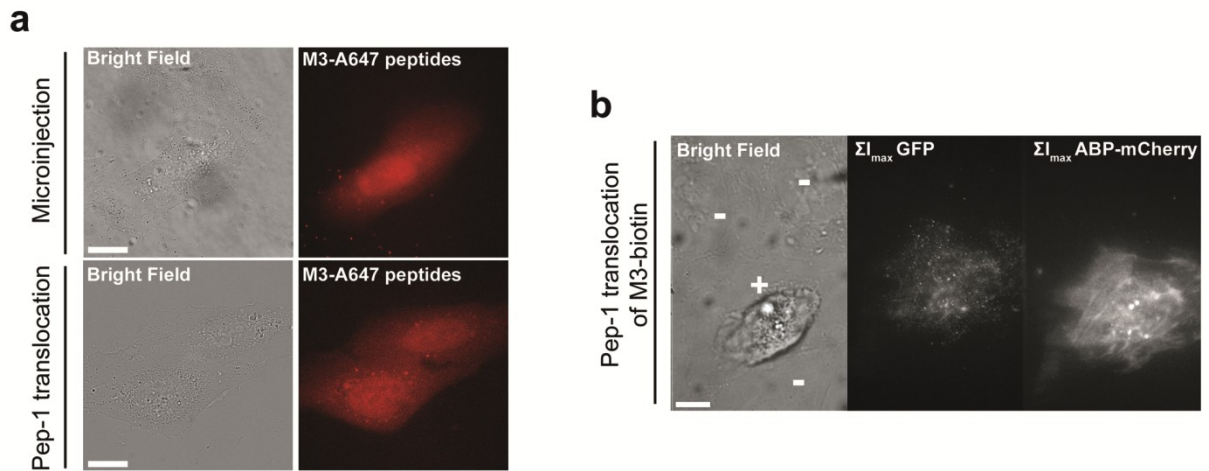
Fig. S8: Intracellular delivery of M3 complementary peptides. (a) M3-A647 peptide conjugates are microinjected (top) or translocated to the cytoplasm of living U2OS cells using cell membrane penetrating Pep-1 peptides (bottom). In both cases, fluorescence imaging by wide field shows that M3-A647 peptides are homogenously distributed throughout the cytoplasm and even diffuse in the cell nucleus. Scale bars: 10 μm. (b) Using Pep-1 carriers, M3-biotin complementary peptides are efficiently translocated to the cytoplasm of a cav1-GFP 1-10$_{(h)}$ expressing U2OS cell (+) identified by its co-expression of ABP-mCherry. The specific punctuated GFP signal observed by TIRF imaging only for the expressing cell, indicates that the translocated M3-biotin peptide are effectively released in the cell cytoplasm where they can complement the plasma membrane-associated cav1-GFP 1-10$_{(h)}$. GFP and ABP-mCherry TIRF images are pixel-based maximum intensity projection images (ΣI_{max}) for all frames of a short dual-color video. Scale bar: 5 μm.
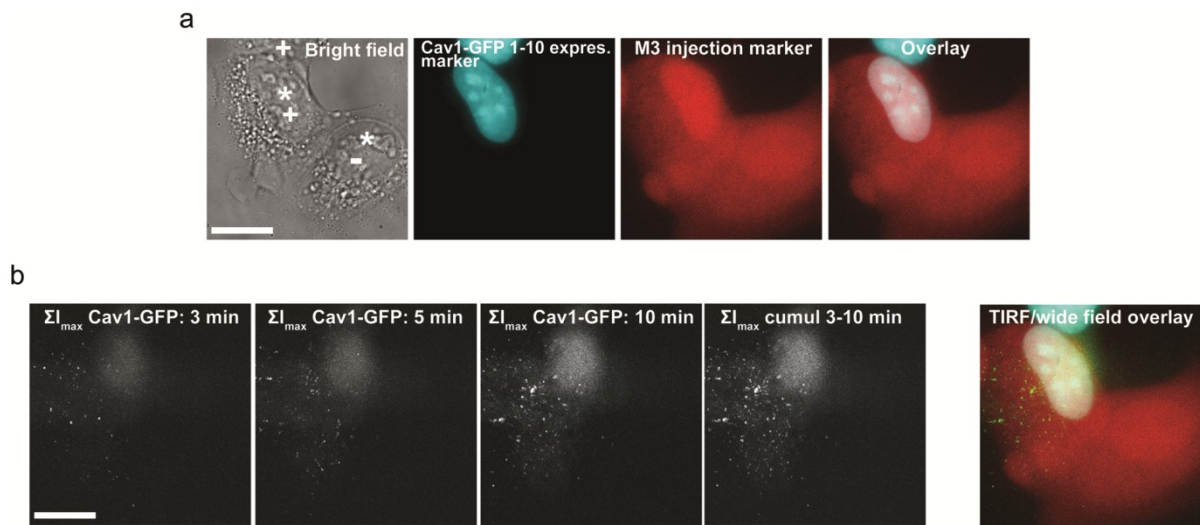
Fig. S9

Fig. S9: Intracellular single biomolecule detection by CALM imaging. (a) U2OS cells expressing cav1-GFP 1-10$_{(h)}$ are identified by wide field fluorescence using the nucleus-localized CFP-LacI-NLS co-expression marker (+). An expressing and a non-expressing cell (-) are both microinjected with biotin-M3 complementary peptides together with a biotin-Alexa 647 injection marker (*). Both cells are then imaged by TIRF for GFP fluorescence. Scale bar: 10 μm. (b) Pixel-based maximum intensity projection (ΣI_{max}) TIRF images of all complemented cav1-GFP$_{(h)}$ detected at the ventral intracellular plasma membrane for both cells in (a). TIRF imaging is performed at 3, 5 and 10 minutes after peptide injection, each time for a 30 seconds long acquisition (frame rate of 60 ms/frame). The overlay of the cumulative 3-10 minutes maximum intensity projection TIRF image with the wide-field image shows that no GFP is detected in the non-expressing cell although it has been microinjected. Scale bar: 10 μm.
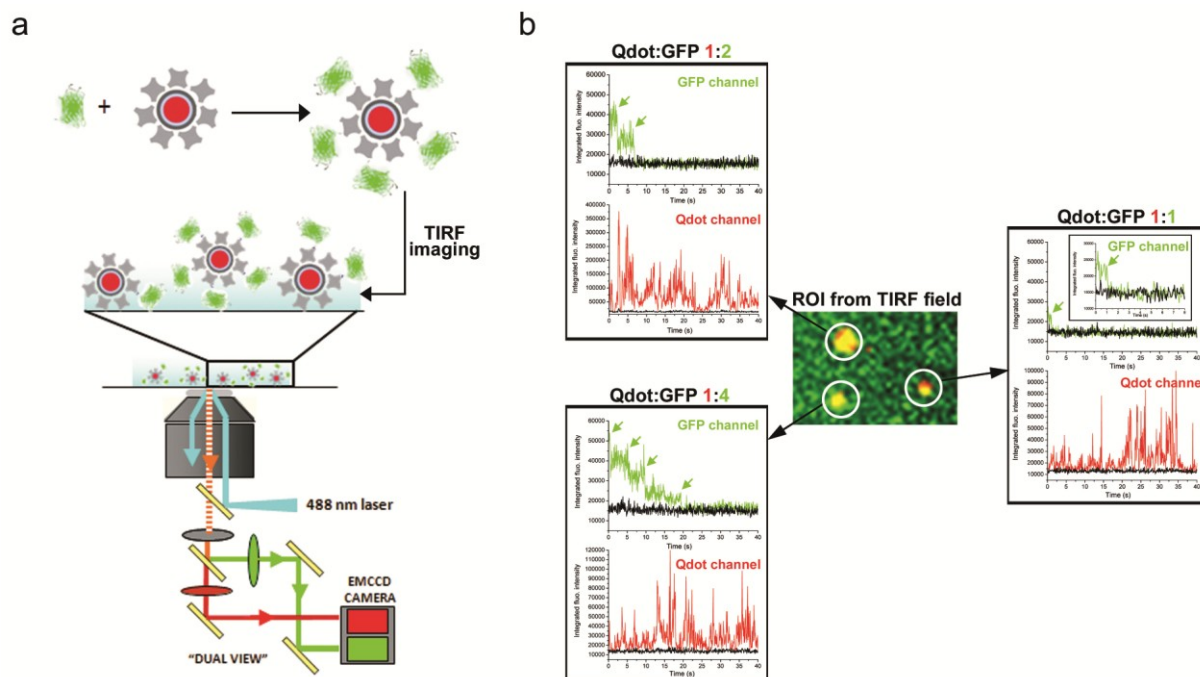
Fig. S10

Fig. S10: *In vitro* coincident single molecule TIRF imaging of complemented split-GFPs on individual quantum dots. (a) Commercial streptavidin qdots (Qdot® 655 streptavidin, Invitrogen) diluted at 50 pM are incubated for 30 min with HPLC purified complemented GFP-biotin (see methods), and are further diluted to single molecule concentrations on clean glass coverslips before being imaged by TIRF. GFP and qdots are simultaneously excited at 488 nm, and their fluorescence is simultaneously recorded on two sides of an EMCCD camera using a dual-view system. (b) After image alignment, both detection channels are overlaid and fluorescence intensity time traces from the qdot and the GFP channel are obtained by integrating fluorescence intensity within a 3x3 pixel area centered on the point spread function of each qdot. The typical blinking pattern of single qdots is observed in the red channel, while sequential photobleaching steps of multiple GFPs bound to individual qdots is often seen in the green channel, consistent with the presence of ~ 5 to 10 streptavidins per qdots (and 20 to 50 potential biotin-binding sites). For streptavidin-Qdot-655 functionalized with a low amount of complemented GFP-biotin, the number of biotin-GFP per qdot can be estimated by counting single GFP bleaching steps. Ratio of 1:2, 1:4 and 1:1 Qdot:GFP are presented here, indicating that even a single copy of GFP attached to a single qdot can be detected.

Fig. S11
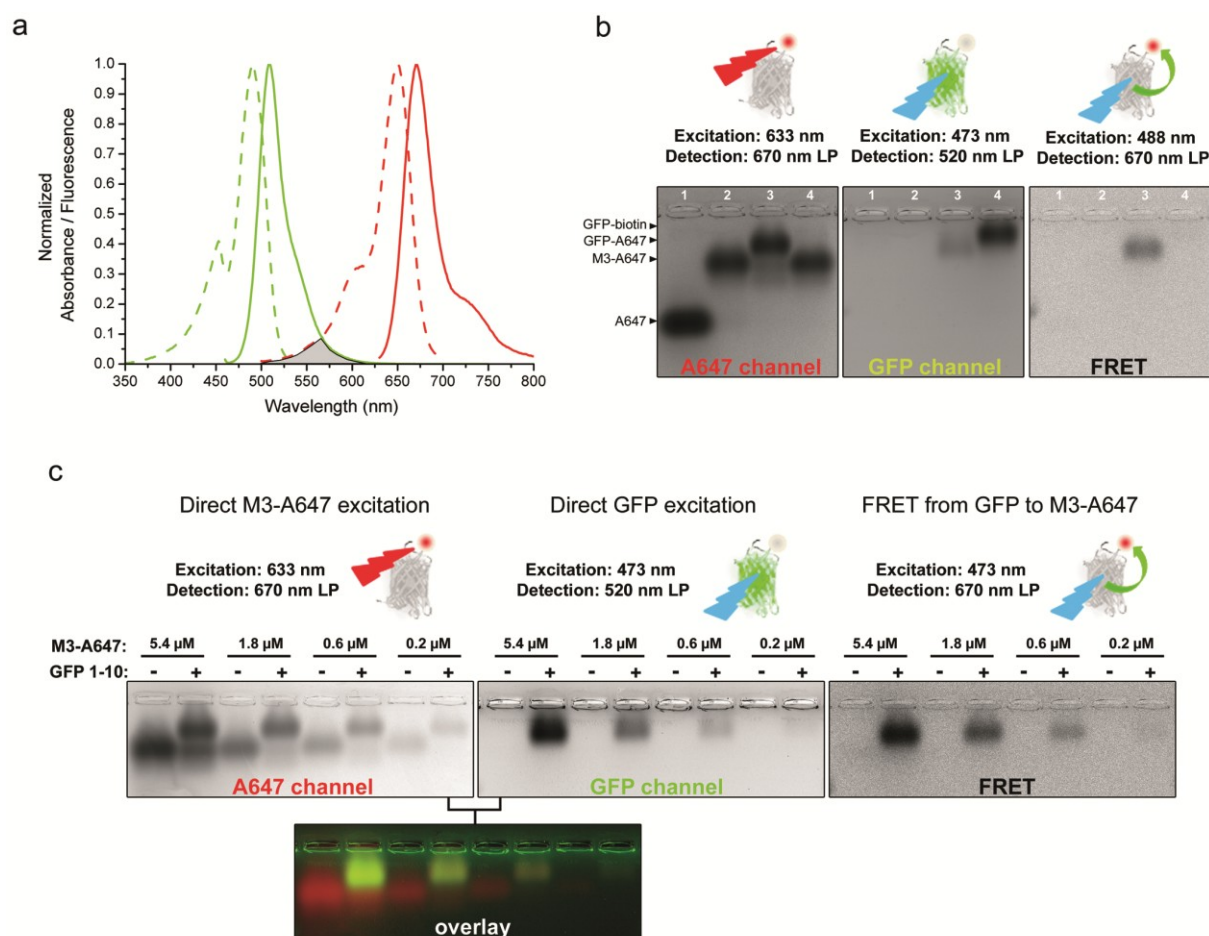
Fig. S11: Complementation-induced Förster resonance energy transfer. (a) Absorption (dash) and emission spectra (line) of complemented split-GFP (green) and M3-A647 peptide conjugate (red). The grey area corresponds to spectral overlap between the emission band of GFP and the absorption band of M3-A647. FRET R_0 for A647-GFP complexes is 3.6 nm. (b) Gel shift assay of figure 1c presented with separated A647, GFP and GFP to M3-A647 FRET channels. (c) Gel shift assay of M3-A647 peptide binding to soluble GFP 1-10. Decreasing concentrations of M3-A647 (5.4, 1.8, 0.6 and 0.2 µM) are incubated with GFP 1-10 (+, "Fold 'n' Glow" reagent) or TNG buffer (-) as described in Methods. The gel is sequentially imaged for M3-A647, GFP and A647-GFP FRET emission as indicated. The binding of M3-A647 to GFP 1-10 and the complementation are characterized by a slower migration of the M3-A647 peptide band, by the appearance of a GFP fluorescent band that co-localizes with the shifted M3-A647 band, and by FRET from GFP to M3-A647. Note that despite the high concentration of GFP 1-10 used in this assay (135µM), a full shift of the M3-A647 peptide band is only observed at about 1.8 µM of M3-A647, indicating that only 1-2 % of GFP 1-10 in the "Fold 'n' Glow" reagent is reactive to complementation. This might be due to the preparation of this commercial reagent which probably involves denaturation and renaturation steps to prepare soluble GFP 1-10 from bacterial inclusion bodies.

Supplementary table

Table: Diffusion characteristics of split-GFP fusion proteins.

	GFP 1-10-CD4	GFP 1-10$_{(h)}$-GPI	Cav1-GFP 1-10$_{(h)}$
Number of trajectories	147	158	177
^{a}D$_{MSD}$ (μm^2/s)	0.21 ± 0.03	0.37 ± 0.02	0.02 ± 0.003
^{b}D$^1_{Pr2}$ (μm^2/s) (fraction) ^{b}D$^2_{Pr2}$ (μm^2/s) (fraction)	0.29 ± 0.02 (64%) 0.021 ± 0.009 (36%)	0.53 ± 0.03 (69%) 0.036 ± 0.008 (31%)	0.059 ± 0.009 (26%) 0.002 ± 0.001 (74%)
Mean duration (s)	1.22 ± 1.14 s	1.10 ± 1.04 s	0.89 ± 0.67 s
Mean localization uncertainty (nm)	24 ± 4 nm	31 ± 5 nm	14 ± 4 nm

^{a}Diffusion coefficients calculated from ensemble mean square displacements (MSD) analysis. ^{b}Diffusion coefficients calculated from probability distribution of the square displacements (P$_r^2$) analysis.

References

1. Cabantous S & Waldo GS (2006) In vivo and in vitro protein solubility assays using split GFP. *Nature Methods* 3(10):845-854.
2. Pinaud F, King D, Moore HP, & Weiss S (2004) Bioactivation and cell targeting of semiconductor CdSe/ZnS nanocrystals with phytochelatin-related peptides. *J Am Chem Soc* 126(19):6115-6123.
3. Iyer G, Pinaud F, Tsay J, & Weiss S (2007) Solubilization of quantum dots with a recombinant peptide from Escherichia coli. *Small* 3(5):793-798.
4. Pinaud F*, et al.* (2009) Dynamic Partitioning of a Glycosyl-Phosphatidylinositol-Anchored Protein in Glycosphingolipid-Rich Microdomains Imaged by Single-Quantum Dot Tracking. *Traffic* 10(6):691-712.
5. Feinberg EH*, et al.* (2008) GFP reconstitution across synaptic partners (GRASP) defines cell contacts and Synapses in living nervous systems. *Neuron* 57(3):353-363.
6. Gettner SN, Kenyon C, & Reichardt LF (1995) Characterization of beta pat-3 heterodimers, a family of essential integrin receptors in C.elegans. *Journal of Cell Biology* 129(4):1127-1141.
7. Fragoso R*, et al.* (2003) Lipid raft distribution of CD4 depends on its palmitoylation and association with Lck, and evidence for CD4-induced lipid raft aggregation as an additional mechanism to enhance CD3 signaling. *Journal of Immunology* 170(2):913-921.
8. Popik W & Alce TM (2004) CD4 receptor localized to non-raft membrane microdomains supports HIV-1 entry - Identification of a novel raft localization marker in CD4. *Journal of Biological Chemistry* 279(1):704-712.
9. Zolotukhin S, Potter M, Hauswirth WW, Guy J, & Muzyczka N (1996) A "humanized" green fluorescent protein cDNA adapted for high-level expression in mammalian cells. *Journal of Virology* 70(7):4646-4654.
10. Cabantous S, Terwilliger TC, & Waldo GS (2005) Protein tagging and detection with engineered self-assembling fragments of green fluorescent protein. *Nature Biotechnology* 23(1):102-107.
11. Clarke S*, et al.* (2010) Covalent Monofunctionalization of Peptide-Coated Quantum Dots for Single-Molecule Assays. *Nano Letters* 10(6):2147-2154.
12. Thompson RE, Larson DR, & Webb WW (2002) Precise nanometer localization analysis for individual fluorescent probes. *Biophysical Journal* 82(5):2775-2783.
13. Michalet X, Lacoste TD, & Weiss S (2001) Ultrahigh-resolution colocalization of spectrally resolvable point-like fluorescent probes. *Methods* 25:87-102.
14. Michalet X (2010) Mean-square-displacement analysis of single-particle trajectories with localization error: Brownian motion in an isotropic medium. *Physics Review E* 82(4):041914.
15. Schutz GJ, Schindler H, & Schmidt T (1997) Single-molecule microscopy on model membranes reveals anomalous diffusion. *Biophysical Journal* 73(2):1073-1080.
16. Chalfie M (1995) Green Fluorescent Protein. (Translated from English) *Photochem. Photobiol.* 62(4):651-656 (in English).
17. Sakamoto S & Kudo K (2008) Supramolecular control of split-GFP reassembly by conjugation of beta-cyclodextrin and coumarin units. *Journal of the American Chemical Society* 130(29):9574-9582.